OPEN ACCESS

Repository of the Max Delbrück Center for Molecular Medicine (MDC) in the Helmholtz Association

http://edoc.mdc-berlin.de/14998

DULIP: A dual luminescence-based co-immunoprecipitation assay for interactome mapping in mammalian cells

Trepte, P., Buntru, A., Klockmeier, K., Willmore, L., Arumughan, A., Secker, C., Zenkner, M., Brusendorf, L., Rau, K., Redel, A., Wanker, E.E.

NOTICE: this is the author's version of a work that was accepted for publication in the *Journal of Molecular Biology*. Changes resulting from the publishing process, such as peer review, editing, corrections, structural formatting, and other quality control mechanisms may not be reflected in this document. Changes may have been made to this work since it was submitted for publication. A definitive version was subsequently published in:

Journal of Molecular Biology
2015 MMM DD ; 427(21): 3375-3388
doi: 10.1016/j.jmb.2015.08.003
Publisher: Elsevier

© 2015, Elsevier. This work is licensed under the Creative Commons Attribution-NonCommercial-NoDerivatives 4.0 International. To view a copy of this license, visit http://creativecommons.org/licenses/by-nc-nd/4.0/ or send a letter to Creative Commons, PO Box 1866, Mountain View, CA 94042, USA.

DULIP: A DUAL LUMINESCENCE-BASED CO-IMMUNOPRECIPITATION ASSAY FOR INTERACTOME MAPPING IN MAMMALIAN CELLS

Philipp Trepte[a], Alexander Buntru[a#], Konrad Klockmeier[a#], Lindsay Willmore[a], Anup Arumughan[a], Christopher Secker[a], Martina Zenkner[a], Lydia Brusendorf[a], Kirstin Rau[a], Alexandra Redel[a] and Erich E Wanker[a]*

[a] Neuroproteomics, Max Delbrueck Center for Molecular Medicine, Robert-Roessle-Straße 10, 13125 Berlin, Germany

[#] Contributed equally

* Corresponding author, E-mail address: ewanker@mdc-berlin.de, Telephone: +49-30-9406-2157, Fax: +49-30-9406-2552

ABSTRACT

Mapping of protein-protein interactions (PPIs) is critical for understanding protein function and complex biological processes. Here, we present DULIP, a dual luminescence-based co-immunoprecipitation assay, for systematic PPI mapping in mammalian cells. DULIP is a second-generation luminescence-based PPI screening method for the systematic and quantitative analysis of co-immunoprecipitations using two different luciferase tags. Benchmarking studies with positive and negative PPI reference sets revealed that DULIP allows the detection of interactions with high sensitivity and specificity. Furthermore, the analysis of a PPI reference set with known binding affinities demonstrated that both low- and high-affinity interactions can be detected with DULIP assays. Finally, using the well-characterized interaction between Syntaxin-1 and Munc18, we found that DULIP is capable of detecting the effects of point mutations on interaction strength. Taken together, our studies demonstrate that DULIP is a sensitive and reliable method of great utility for

systematic interactome research. It can be applied for interaction screening as well as for the validation of PPIs in mammalian cells. Moreover, DULIP permits the specific analysis of mutation-dependent binding patterns.

HIGHLIGHTS

- DULIP is a dual luminescence-based co-immunoprecipitation assay suitable for systematic analysis of PPIs
- DULIP generates quantitative interaction scores
- DULIP reliably detects PPIs with high sensitivity and specificity
- DULIP measures the effects of point mutations on interaction strength

KEYWORDS

Systematic protein-protein interaction screening; luminescence normalization; quantitative interaction score; detection of low- and high-affinity interactions; disease-mutation detection; quantification of interaction strength; DULIP.

ABREVIATIONS

Protein-protein interaction (PPI); dual luminescence-based co-immunoprecipitation (DULIP); yeast two-hybrid (Y2H); kinase substrate sensor (KISS); single-molecule pull-down (SiMPull); mammalian-membrane two-hybrid assay (MaMTH); luminescence-based mammalian interactome mapping (LUMIER); *Renilla* luciferase (RL); firefly luciferase (FL); Protein A (PA); Gateway cassette (GW); normalized luminescence-based interaction ratio (NIR); background corrected NIR (cNIR); positive reference set (PRS); negative reference set (NRS); affinity-based interaction reference set (AIRS); *Homo sapiens* positive reference set (hsPRS-v1); *Homo*

sapiens random reference set (hsRRS-v1); human integrated protein-protein interaction reference (HIPPIE).

INTRODUCTION

Protein-protein interactions (PPIs) play a crucial role in many biological processes, including cell signaling, gene expression regulation and the trafficking of membrane vesicles [1; 2]. Therefore, the identification and characterization of PPIs is considered an important step towards elucidating the function of complex biological systems as well as the pathobiological mechanisms in diseases [3; 4; 5; 6]. Various yeast two-hybrid and affinity purification-based methods have proven to be successful for the identification and validation of PPIs[5; 7; 8]. Both types of methods yield reliable, largely complementary PPI data sets, which allow the creation of interactome networks involving whole proteomes or particular cellular pathways and disease processes of interest[9; 10; 11; 12; 13; 14; 15].

To this day, systematic mapping of binary interactions between human proteins has been predominantly performed in yeast cells[3; 16; 17; 18]. Despite being highly efficient and previously successful, this approach has the disadvantage of placing human proteins in an artificial environment, which may lead to abnormal protein modifications and increased detection of false positive PPIs[19]. Thus, the development and validation of reliable assays for the identification and systematic screening of human PPIs in mammalian cells are of high importance for advanced interactome research[1; 19].

Several assays for the detection of binary human PPIs based on mammalian cells have been developed in recent years. This includes methods such as KISS [20], SiMPull[21; 22], MaMTH[23] and different variants of the LUMIER assay[24; 25; 26; 27; 28; 29]. All these methods use different molecular principles and readouts for PPI detection.

Among the currently available methods only the LUMIER method (for luminescence-based mammalian interactome mapping) has been applied in systematic, large-scale PPI screening efforts[28; 30; 31]. LUMIER is a luminescence-based co-immunprecipitation assay, in which the *Renilla* luciferase (RL) enzyme is fused to proteins of interest. These RL-tagged fusion proteins are co-expressed with FLAG-tagged fusion proteins in HEK293 cells and interactions are detected by RL enzymatic assays on immunoprecipitates[24]. Although this method is, in principle, suitable for high-throughput PPI mapping in mammalian cells [24], bait protein immunoprecipitation cannot easily be quantified. To overcome this problem, Taipale et al. (2012) have established an antibody-based method to systematically measure the abundance of precipitated FLAG-tagged proteins in LUMIER assays[28].

Here, we present a second generation LUMIER PPI screening assay, which allows quantification of both bait and prey hybrid proteins using two different luciferase tags. DULIP (for dual luminescence-based co-immunoprecipitation assay) detects PPIs between protein A-(PA)-RL-tagged bait and firefly luciferase (FL)-tagged prey proteins in mammalian cells. Benchmarking studies with positive and negative reference sets revealed that DULIP is a powerful interaction screening method, which enables the detection of human PPIs with high sensitivity and specificity. Furthermore, DULIP can detect both low- and high-affinity interactions as well as the effects of point mutations on interaction strength. We suggest that DULIP is suitable for both systematic screening and validation of PPIs in mammalian cells. Potential applications of the method are discussed.

RESULTS

To establish a **du**al **l**uminescence-based co-**i**mmuno**p**recipitation (DULIP) interaction detection assay, we first constructed the Gateway-compatible plasmids pPA-RL-GW and pGW-RL-PA, from which bait proteins with N- or C-terminal protein-A-*Renilla* luciferase (PA-RL) tags are expressed (Fig. 1a). Similarly, we constructed pFL-V5-GW and pGW-FL-V5 plasmids for the expression of prey proteins harboring N- or C-terminal firefly luciferase (FL) tags.

Next, cDNA fragments encoding bait or prey fusion proteins were inserted in the available plasmids for systematic interaction testing. For proof-of-principle experiments, we selected the proteins BAD and BCL2L1 because these proteins were previously shown to interact in various PPI detection assays[32; 33]. Using the Gateway cloning technology, we generated plasmids encoding the proteins PA-RL-BAD (bait) and FL-BCL2L1 (prey) (Fig. 1b Table S1). Additionally, we constructed plasmids encoding the fusion proteins PA-RL-mCherry and FL-mCherry for control experiments. We hypothesized that an unrelated monomeric protein like mCherry should not specifically interact with BAD or BCL2L1 in co-immunoprecipitation experiments. Therefore, fusions with mCherry might be generally useful to assess non-specific interactions of tested bait and prey fusion proteins. To address the lack of data normalization in luminescence-based PPI assays[34], which accounts for a high variability between experimental replicates, we additionally generated a tandem construct that encodes a PA-RL-FL hybrid protein (Fig. 1b). In this fusion protein FL is connected via a short peptide linker to the PA-RL fragment. The identities of the generated plasmids as well as their encoded hybrid proteins are summarized in Table S1.

DULIP assays facilitate the detection of the known interaction between BAD and BCL2L1

To study the interaction, we performed four independent transfections of HEK293 cells in 96-well microtiter plates (Fig. 2a). This included the analysis of the protein pairs PA-RL-BAD/FL-BCL2L1, PA-RL-BAD/FL-mCherry (control 1) and PA-RL-mCherry/FL-BCL2L1 (control 2) as well as the investigation of the hybrid protein PA-RL-FL (control 3). Transfected cells were lysed after 48 h and both RL and FL enzymatic activities (RL_{IN} and FL_{IN}) were quantified in crude protein extracts. We were able to measure RL and FL activities in all four cell lysates (Fig. 2b), suggesting that the expected recombinant hybrid proteins were indeed produced in the cells. Next, the PA-tagged bait proteins were immunoprecipitated from cell lysates using IgG-coated 384-well microtiter plates. After extensive washing the enzymatic activities of both RL and FL were quantified (RL_{OUT} and FL_{OUT}) in precipitated protein complexes. In this step, the measured RL activities indicate the successful immunoprecipitation (IP) of PA-tagged bait proteins, while the measured FL activities are indicative of the co-precipitated prey proteins (CoIP, Fig. 2a and 2c). In all four experiments, which were performed in parallel, the expected PA-tagged bait proteins were immunoprecipitated. However, high FL_{OUT} activities were only measured for the tandem construct PA-RL-FL and the prey protein FL-BCL2L1 that was co-precipitated with the bait protein PA-RL-BAD (Fig. 2c). For the interaction of interest PA-RL-BAD/FL-BCL2L1 in comparison to the control interactions PA-RL-BAD/FL-mCherry and PA-RL-mCherry/FL-BCL2L1 a ~7- and a ~292-fold higher luciferase activity (FL_{OUT}) was obtained, indicating that the method is suitable to distinguish between a proven PPI (BAD and BCL2L1) and negative control PPIs (e.g. PA-RL-BAD/FL-Cherry). These results also confirm mCherry as a useful control protein that

can be applied more generally in DULIP assays to investigate non-specific background binding.

As the co-immunoprecipitation efficiency of prey proteins depends on the immunoprecipitation efficiency of PA-tagged bait proteins, we calculated the luciferase activity ratios (FL_{OUT}/RL_{OUT}) for the interactions PA-RL-BAD/FL-BCL2L1, PA-RL-mCherry/FL-BCL2L1 and PA-RL-BAD/FL-mCherry. In addition, the FL_{OUT}/RL_{OUT} ratio was determined for the control protein PA-RL-FL. This ratio - termed luciferase immunoprecipitation ratio (LIR) of control 3 - was subsequently utilized to normalize the luciferase activity ratios of the tested bait/prey combinations (interaction of interest and controls 1 and 2, see Fig. 2a). This revealed the **n**ormalized luminescence-based **i**nteraction **r**atios (NIRs, Fig. 2d) for the three tested interactions. NIRs indicate the success of prey protein co-immunoprecipitation in relation to the efficacy of bait protein immunoprecipitation. As shown in Fig. 2d, the calculated NIR for the interaction PA-RL-BAD/FL-BCL2L1 is 185- and 203-fold higher than the NIRs for the control interactions PA-RL-BAD/FL-mCherry and PA-RL-mCherry/FL-BCL2L1, respectively. Thus, our normalization step significantly increases the specificity of PPI detection, allowing a clear distinction between positive and negative PPIs.

Finally, we calculated a background **c**orrected **n**ormalized luminescence-based **i**nteraction ratio (cNIR, Fig. 2d) for PA-RL-BAD/FL-BCL2L1. We first compared the NIRs obtained for the control PPIs PA-RL-BAD/FL-mCherry and PA-RL-mCherry/FL-BCL2L1 and identified the interaction with the higher value. Next, this value, here the NIR for the interaction PA-RL-BAD/FL-mCherry, was subtracted from the NIR of the interaction of interest, PA-RL-BAD/FL-BCL2L1. In the following systematic investigations of PPIs with DULIP assays cNIRs will be utilized as a quantitative measure in order to compare interaction data (see below). A detailed

step-by-step description of the calculations that lead to cNIRs can be found in the supplemental information (Fig. S1).

Y2H and FRET assays confirm the interaction between BAD and BCL2L1

First, we employed an established yeast two-hybrid (Y2H) interaction-mating assay[3; 16] to examine the interaction between BAD and BCL2L1. We generated MATa yeast strains expressing the bait proteins LexA-BAD or LexA-mCherry and subsequently mated these strains on YPD plates with MATα strains expressing the prey proteins Gal4-BCL2L1 or Gal4-mCherry. Next, the generated diploid yeast strains were spotted onto selective plates; PPIs were identified through monitoring of yeast colony growth (Fig. S2a). For each tested interaction, 12 independent matings and three technical replicates were performed. We detected the interaction between LexA-BAD and Gal4-BCL2L1 in all mating experiments (100%, Fig. 3b), confirming the results of the DULIP assay (Fig. 2d). In strong contrast, the control PPIs LexA-BAD/Gal4-mCherry and LexA-mCherry/Gal4-BCL2L1 were detected with significantly lower frequency (Fig. S2b), indicating that the Y2H method is capable of distinguishing between specific and non-specific PPIs.

Finally, we also examined the interaction between BAD and BCL2L1 in mammalian cells using a sensitive FRET assay (Fig. S2c). In these experiments ECFP- and EYFP-tagged fusion proteins were co-produced in HEK293 cells and FRET efficiencies were determined using the sensitized emission method[35; 36]. For data comparison the hybrid fusion protein ECFP-EYFP was used as a positive control. It routinely showed FRET efficiencies of ~40% in various transfection experiments (Fig. S2c). In strong contrast, in cells co-producing the control proteins ECFP and EYFP only very low FRET values were obtained. However, we detected relatively high FRET efficiencies (~38%) in cells co-expressing the proteins ECFP-

BAD/EYFP-BCL2L1 (Fig. S2c), confirming the results of Y2H and DULIP assays. As additional controls, we also examined the interactions ECFP-BAD/EYFP and ECFP/EYFP-BCL2L1, indicating that the fluorescent proteins EYFP and ECFP do not unspecifically interact with the tested proteins of interest.

Assessment of assay quality

To assess assay quality parameters such as sensitivity and specificity[8; 20] reference sets of positive and negative interacting pairs are required. To compile a positive reference set (PRS) of human PPIs we started with 181 interactions that possess a PPI confidence score of ≥0.99 in the HIPPIE database[37]. PPIs with such scores are considered as high confidence interactions, because they were previously shown to be detectable with multiple independent methods in various experiments[37]. From this PPI set, 25 protein pairs were randomly selected, of which 23 were finally examined in interaction tests (Fig. 3a and Table S2). To compile a negative reference set (NRS) we started with 114 PPIs from the Negatome database (v1.0). These interactions were not detectable with at least three independent methods in previous studies[38], suggesting that they should also not be identified in DULIP assays. We randomly selected 30 protein pairs from this data set for systematic PPI analysis in mammalian cells (Fig. 3b, Table S3).

Next, two expression plasmids were constructed for each selected protein, enabling its investigation either as a bait (PA-RL-tagged fusion) or as a prey (FL-tagged fusion) in DULIP assays. Thus, all selected protein pairs were systematically analyzed as bait/prey (set **a** of reference PPIs) and prey/bait combinations (set **b** of reference PPIs) in mammalian cells (Tables S2 and S3). In total, 95 protein pairs

(PRS and NRS) were systematically tested in two independent experiments (experiment 1 and 2) in DULIP assays (Fig. S3a).

As described above for the interaction between BAD and BCL2L1 (Fig. 2a-d), we performed four independent transfections in order to analyze a PPI of interest. In all these experiments, after cell lysis, both RL and FL activities were systematically quantified in protein extracts before and after co-immunoprecipitation of protein complexes. At this stage the obtained FL_{OUT} values for all PPIs of interest, which indicate the efficiency of the co-immunoprecipitation, were divided by FL_{OUT} values of control PPIs (controls 1 and 2, see Fig. 2a and Fig. S1) in order to obtain FL_{OUT}-based interaction control ratios (ICRs). Only PPIs with ICRs of ≥3 (see step 3 in Fig. S1) were considered for further analysis. This selection criterion was defined for systematic large-scale PPI detection studies to ensure that the FL_{OUT} values for all tested PPIs of interest are significantly higher than the FL_{OUT} values of the respective control PPIs (controls 1 and 2). Through this selection strategy 30 interactions in the NRS and 7 in the PRS were excluded from further analysis.

As the production of prey proteins is critical for the success of co-immunoprecipitation experiments, we next assessed the abundance of these proteins (FL fusions) in all prepared protein extracts. We used the frequency distribution and a fitted Gaussian function of all measured FL_{IN} values to identify prey proteins that are not sufficiently produced in HEK293 cells (Fig. S3b). Prey proteins with FL_{IN} values $<\mu-3\sigma$ were defined as not expressed and not considered for further data analysis. With this strategy, all of the interactions in the reference interaction sets (PRS and NRS) were considered for benchmarking studies (Fig. S3a).

Next, we used a similar strategy to assess the immunoprecipitation of bait proteins (PA-tagged fusions) as a prerequisite for the successful co-immunoprecipitation of prey proteins (Fig. S3c). Thus, PPIs with bait proteins that are

not sufficiently precipitated should not be considered for further data analysis. Using a fitted Gaussian function we defined 3 bait proteins with RL_{OUT} values <μ-3σ (Fig. S3a). 5 PPIs harboring these bait proteins were excluded from further benchmarking studies.

For the remaining 53 PPIs the corrected normalized luminescence-based interaction ratios (cNIRs), a quantitative measure of the potential interaction strength of proteins, were calculated (Fig. S4 a-d). We found that the cNIRs for the tested PPIs were highly reproducible in two independent DULIP experiments (r^2 = ~0.98; Fig. 3c). Moreover, they covered a broad range of values, suggesting that the method detects PPIs with different binding affinities. We next used the ROC (receiver operating characteristic) analysis (Fig. 3d) to define the cutoff for the identification of "true" positive PPIs. Using a cNIR of 3 we observed a clear separation between known positive and potential false-positive PPIs. Thus, a cNIR cutoff of ≥ 3 was utilized to estimate the assay sensitivity. Under these conditions, 79.5% of the PPIs in the PRS were detected with the DULIP assay (Fig. 3e), while 3.3% of the PPIs in the NRS were identified. The results of the benchmarking studies are summarized in Fig. 3f and 3g.

To more comprehensively evaluate the performance of DULIP, we next examined the assay's detection rate of PPIs in the established reference sets hsPRS-v1 and hsRRS-v1, which were successfully applied previously to benchmark various PPI detection methods[8; 20; 39]. Like for the PPIs in the initially tested reference sets (Fig. 3a and b) all selected protein pairs were systematically analyzed as bait/prey and prey/bait combinations in mammalian cells (Fig. S5a and b). In these experiments, we detected PPIs in the positive reference set hsPRS-v1 and the random reference set hsRRS-v1 with a success rate of 35.4 and 3.7%, respectively

(Fig. 3e and Fig. S5 and S6), confirming that the established DULIP assay is a robust method, which allows the detection of PPIs with high sensitivity and specificity.

DULIP allows the detection of both low- and high-affinity interactions

To address the question whether DULIP can detect both low- and high-affinity PPIs, we additionally created an affinity-based interaction reference set (AIRS). It exclusively consists of interactions with known dissociation constants (K_{ds}). To generate an AIRS, we selected PPIs from PDBind[40] as well as from the PPI Affinity Database 2.0[41] and subsequently subcloned cDNAs encoding potential bait and prey fusion proteins into DULIP expression plasmids. In total, 57 affinity-based interactions were selected which were systematically tested as bait/prey and prey/bait combinations in DULIP assays (Fig. 4a). As shown in Fig. 4b, the selected interactions in AIRS indeed covered a broad spectrum of binding affinities, including both low- (59% of PPIs with a K_d <100 nM) and high-affinity (41% of PPIs with a K_d >100 nM) interactions. Using assay conditions identical to the ones applied for hsPRS-v1 and hsRRS-v1 (Fig. 3e), we detected interactions in AIRS with a success rate of 29.8% (17 of 57 tested PPIs). Strikingly, besides strong PPIs (K_d values in the nanomolar range), also relatively weak interactions (K_d values in the micromolar range) could be readily detected (Fig. 4c and d), supporting the hypothesis that both high- and low-affinity interactions can be identified with DULIP. However, our experiments clearly demonstrate that DULIP is more likely to detect higher affinity than lower affinity PPIs (Fig. 4c and d), substantiating previous observations that co-immunoprecipiation-based PPI detection methods have a certain bias for stronger interactions[42].

Next, we examined whether the published binding strengths (defined through K_d values) of PPIs in the AIRS correlate with calculated cNIR values obtained with DULIP assays (Tab. S5). As shown in Fig. 4e, we found a significant correlation between published K_d values and luminescence-based cNIRs, supporting the hypothesis that high cNIRs are an indication of strong interactions.

Point mutations influence the detection of PPIs with DULIP assays

Previous studies indicate that point mutations in proteins influence their binding affinities, which can be monitored with Y2H assays or other interaction detection methods[18; 43]. Therefore, we examined whether the DULIP assay can detect the effect of mutations on the well-described interaction between the synaptic proteins Munc18 and Syntaxin-1[44; 45; 46]. Previous studies have demonstrated that point mutations in Munc18 reduce its binding affinity for the protein Syntaxin-1 (Fig. 5a and b), suggesting that such effects on interaction strength should also be detectable with DULIP assays. To address this question we co-produced the bait protein PA-RL-Syntaxin-1 with the prey proteins FL-Munc18-wt, FL-Munc18-K46E, FL-Munc18-E59K or FL-Munc18-K46E/E59K in HEK293 cells and determined cNIRs for these PPIs. We found that the interaction between PA-RL-Syntaxin-1 and FL-Munc18-wt can be readily detected with DULIP assays (Fig. 5c), confirming previously published results[44; 45; 46]. However, the interactions between PA-RL-Syntaxin-1 and the mutant proteins FL-Munc18-K46E, FL-Munc18-E59K and FL-Munc18-K46E/E59K were not identifiable. This demonstrates that the effects of both single and double point mutations on interaction strength can be monitored using standard DULIP assays.

Finally, we examined whether the point mutations in Munc18 influence its association with Syntaxin-1 in an established Y2H interaction assay[3; 16] (Fig. 5d and e). We observed that the hybrid protein pairs Gal4-Syntaxin-1/LexA-Munc18-wt, Gal4-Syntaxin-1/LexA-Munc18-K46E and Gal4-Syntaxin-1/LexA-Munc18-E59K interact in Y2H assays. However, the interaction between Gal4-Syntaxin-1 and LexA-Munc18-K46E/E59K was not detected. This suggests that Y2H colony growth assays are less sensitive for the detection of subtle changes in affinity due to single point mutations than DULIP assays. However, more comprehensive studies with multiple mutant proteins are necessary to further substantiate these results.

DISCUSSION

In this study, we have established and benchmarked a dual luminescence-based co-immunoprecipitation method – termed DULIP – that can be applied for systematic PPI mapping in mammalian cells. The method is an advancement of the previously described LUMIER method, which allows the detection of PPIs through quantification of luminescence activity after immunoprecipitation[28; 47]. Classical LUMIER assays have the disadvantage that bait protein immunoprecipitation cannot be quantified in systematic co-immunoprecipitation experiments. To overcome this limitation a modified LUMIER assay (LUMIER with BACON) enabling the quantification of precipitated FLAG-tagged bait proteins with additional ELISAs was recently developed[28]. This method is clearly an improvement of the initially described LUMIER assay. Through the application of LUMIER with BACON a large number of novel client proteins interacting with the molecular chaperone Hsp90 have been successfully identified[28]. Furthermore, the method more recently helped to establish a comprehensive quantitative chaperone interaction network revealing the architecture of protein homeostasis pathways[31]. For systematic mapping of PPIs on a proteome-wide scale with LUMIER with BACON, however, the quantification of bait proteins is achieved through ELISAs, which need to be performed in addition to luciferase assays. This is labor intensive and requires additional resources, which is a drawback, especially in high-throughput application of the procedure.

To overcome these limitations we have developed DULIP, which enables the quantification of co-immunoprecipitated bait and prey proteins in a single sample. This is achieved through the co-expression of two luciferase-tagged proteins in mammalian cells: a *Renilla* luciferase (RL) fusion (bait) and a firefly luciferase (FL) fusion (prey) protein. Both can be quantified in the same reaction by using chemistries that allow the separate measurement of each luciferase. Thus, DULIP

assays are superior when large numbers of PPIs are to be systematically tested in mammalian cells with co-immunoprecipitations.

A limitation of luminescence-based PPI methods is that data output is often highly variable and that assays performed on different days and in different microtiter plates yield quantitatively inconsistent results. This inter- and intra-assay variability is most probably due to the fact that the assay conditions like temperature, incubation time, transfection efficiency etc. cannot be controlled perfectly in repeated experiments and that small changes in the concentrations of transiently transfected plasmids have a high impact on protein expression and therefore on luminescence activity. To overcome these limitations it is important to standardize the different steps of the PPI screening procedure and to include controls which can be used for data normalization on each assay plate. We found that the luminescence values, which were obtained with the control protein PA-RL-FL (Fig. 2b and c), are suitable for normalization of the luminescence output of tested PPIs. Through this normalization step and the calculation of background corrected normalized interaction ratios (cNIRs) for all tested PPIs, highly reproducible, quantitative interaction data were obtained (Fig. 3c), which can be directly compared between experiments. We suggest that the control protein PA-RL-FL could be used more generally for normalization of measured luminescence activities in order to produce widely comparable, quantitative PPI data.

In a recently reported study a pull-down PPI detection method with two luciferase tagged fusion proteins has been described[26]. In strong contrast to DULIP, streptavidin beads are utilized for the precipitation of biotinylated HAVI-tagged bait proteins. This has the disadvantage that initially a biotin ligase is required, which needs to be additionally co-produced in mammalian cells. However, biotin ligases are known to be of low specificity for their targets[48]. Besides the bait protein, the

potentially interacting prey protein might also be biotinylated. However, this previously reported method has not yet been systematically benchmarked with well-defined PPI reference sets. It remains to be seen whether it is suitable for larger scale application and the generation of quantitative PPI data.

Our studies with a positive PPI reference set composed of high-confidence PPIs from the HIPPIE database (selected PPIs with a HIPPIE score of ≥0.99) revealed that benchmarked DULIP assays (cNIR cutoff ≥3) can detect known human PPIs with a sensitivity of ~79.5% (Fig. 3e). This was a surprisingly high, unexpected PPI detection rate as many previously published PPI detection assays recovered binary interactions from positive reference sets with success rates of 20-35%[8; 20]. We therefore performed an additional assessment of the method's sensitivity using the hsPRS-v1 reference set, which has already been applied for the benchmarking of multiple PPI detection methods[8; 20; 39]. Interestingly, positive PPIs were recovered from hsPRS-v1 with a success rate of ~35% (Fig. 3e), which is in good agreement with many previously published studies. Thus, our benchmarking studies with hsPRS-v1 and hsRRS-v1 indicate that DULIP performs similarly well as other previously described PPI detection methods like LUMIER[8; 20]. This is also supported by our studies with a newly generated affinity-based interaction reference set, AIRS, which contains a broad spectrum of lower and higher affinity interactions (Fig. 4a). We found that DULIP assays can detect PPIs in AIRS with a sensitivity of ~30% (Fig. 4c and d), which is in agreement with the hsPRS-v1 results and previously published data. The reason for the very high recovery of PPIs from the PRS (Fig. 3e) is still unclear. We suggest that the PRS compared to the hsPRS-v1 is enriched for high-affinity interactions, which probably have a higher tendency to yield a positive score in a variety of different experimental systems. Nevertheless, our investigations of

various PPI reference sets indicate that DULIP is a very robust method, which allows the detection of PPIs with high sensitivity and specificity.

The generation of AIRS, which exclusively contains PPIs with published dissociation constants also allowed us to assess whether the quantitative luminescence-based output values (cNIRs) of DULIP assays provide an indication of interaction strength. Using PPIs from AIRS, we found a positive correlation between cNIRs and published K_d values (Fig. 4e), indicating that the binding strength of interactions indeed influences the output of DULIP assays. Thus, the detection of PPIs with high cNIRs suggests that relatively stable protein complexes are formed in mammalian cells. However, more detailed validation studies with biochemical and biophysical methods are necessary to further substantiate the results obtained with DULIP.

Several lines of experimental evidence indicate that mutations changing the amino acid composition of proteins (missense point mutations and in-frame insertions or deletions) can influence their binding affinity[43; 45; 49]. To reliably monitor such mutation-dependent effects quantitative PPI detection methods are required. Here, we examined whether DULIP assays are capable of detecting the influence of point mutations on interaction strength. We focused our efforts on the well-characterized interaction between Munc18 and Syntaxin-1, which plays a functional role in synapse communication[44; 45; 46]. Previous biochemical studies have demonstrated that the point mutations K46E and E59K decrease the binding affinity of this interaction[45], suggesting that such a reduction should also be detectable with DULIP assays. Strikingly, our studies confirmed the effect of K46E and E59K on the interaction between Munc18 and Syntaxin-1 (Fig. 5c), indicating that the method is well-suited for monitoring the impact of point mutations on interaction strength with high potential for the investigation of disease-causing mutations.

We propose that DULIP is a highly valuable method for the identification of PPIs in mammalian cells. It can be applied for high-throughput PPI screening as well as for the validation of PPIs identified with other methods such as the Y2H system[8; 15]. DULIP assays are suitable for the quantitative analysis of PPIs, enabling the detection of PPIs with different interaction strengths and the analysis of the impact of mutations, therapeutic molecules or posttranslational modifications on the association of proteins.

MATERIALS & METHODS

Plasmid construction

DULIP vectors pPA-RL-GW and pFL-V5-GW for the production of N-terminal fusions were described previously[50]. For the generation of vectors encoding C-terminal fusion proteins the sequences coding for *Renilla* luciferase (RL) and protein A (PA) were amplified from pPA-RL-GW with primers 5'-GCTGTAAAGCTTATGGCTTCCAAGGTGTACG-3', 5'-GCTGTAGAATTCCTGCTCGTTCTTCAGCAC-3' (RL), 5'-GCTGTAGAATTCGGCTCGGGCTCGATGGTGGACAACAAATTCAAC-3' and 5'-GCTGTACTCGAGTCACGAGTTCGCGTCTACTTTC-3' (PA). The resulting PCR fragments were cloned simultaneously in pcDNA3.1(+) (Invitrogen) via HindIII/EcoRI/XhoI restriction sites to obtain pRL-PA. Firefly-V5 cDNA was PCR amplified from pFL-V5-GW with primers 5'-GCTGTAAAGCTTATGGAAGACGCCAAAAACATAAAG-3' and 5'-GCTGTACTCGAGTCACGTAGAAT CGAGACCGAGGAG-3' and cloned in pcDNA3.1(+) via HindIII/XhoI restriction sites to obtain pFL-V5. Subsequently, the Gateway cassette (GW) was PCR-amplified from pBTM116-D9[3] and cloned into pReni-PA and pFire-V5 using NheI/HindIII restriction sites, resulting in pGW-RL-PA and pGW-FL-V5. The plasmid pdECFP-C1 was kindly provided by Dr. Stefan Wiemann (DKFZ). The plasmid pdEYFP-C1 was obtained from a commercial supplier (ImaGenes). As the gateway destination vectors that contain no insert but the gateway cassette show a weak expression in HEK293 cells, we removed the gateway cassette from the vectors pdEYFP-C1 and pdECFP-C1. An oligonucleotide adaptor 5'-ATAAGTGGCCGGCCACT-3' was self-annealed and cloned into pdEYFP-C1 and pdECFP-C1 via BspEI/XbaI restriction sites to obtain pdEYFP and pdECFP.

For generation of pPA-RL-mCherry, pFL-mCherry and pPA-RL-FL, the coding sequence of mCherry was amplified from pmCherryGW[27] (Invitrogen) and the firefly luciferase coding sequence from pFL-V5-GW. For cloning of mCherry the primers 5'-GGGGACAAGTTTGTACAAAAAAGCAGGCTTCATGGTGAGCAAGGGCGAGGAGGATAAC-3' and 5'-GGGGACCACTTTGTACAAGAAAGCTGGGTCCTTGTACAGCTCGTCCATGCCG-3' and for the firefly luciferase 5'-GGGGACAAGTTTGTACAAAAAAGCAGGCTTCGCCACCATGGAAGACGCCAAAAAC-3' and 5'-GGGGACCACTTTGTACAAGAAAGCTGGGTCCACG GCGATCTTTCCGCCCTTC-3' were used. To generate a Syntaxin-1 fragment that lacks the Syntaxin-1 transmembrane domain the primers 5'-GGGGACAAGTTTGTACAAAAAAGCAGGCTTCATGAAGGACCGAACCCAGGA-3' and 5'-GGGGACCACTTTGTACAAGAAAGCTGGGTCCGCCTTGCTCTGGTACTTG-3' were used for PCR amplification (1-261 aa, Syntaxin-1ΔTM) from the entry clone RZPDo834H065D. The resulting PCR fragments were shuttled into pDONR221 (Invitrogen) with the BP clonase (Invitrogen) to generate entry plasmids that can be used for shuttling into destination plasmids. To introduce the single and double point mutants K46E and E59K into Munc18, the 5'-phosphorylated primers 5'-ATGACAGACATCATGACCGAGG-3' and 5'-CTCGCAGCAGGAGGACAGCATC-3' (K46E) as well as 5'-GATATCAACAAGCGCCGAGAGC-3' and 5'-CTTCACAATTGTGATGCCCTCG-3' (E59K) were used for PCR amplification. The Munc18 wild-type cDNA from the pENTRZ-Munc18 construct that was kindly provided by Prof. Dr. Matthijs Verhage (Vrije Universiteit). The resulting entry vectors harboring the genes encoding the proteins Munc18-wt, Syntaxin-1, BAD and BCL2L1 were utilized to generate the plasmids pPA-RL-GW, pFL-V5-GW, pBTM116-D9, pACT4-DM, pdEYFP-C1 and pdECFP-C1 using the LR clonase. Similarly, the

cDNAs encoding the proteins for the MDC positive and negative reference sets (Tab. S2 and S3), the CCSB reference sets (Tab. S4) as well as AIRS (Tab. S5) were shuttled into the vectors pPA-RL-GW, pGW-RL-PA, pFL-V5-GW or pGW-FL-V5 using the LR clonase.

Cell culture and transfection

The human embryonic kidney cell line 293 (HEK293) was grown in DMEM supplemented with 10% heat inactivated fetal bovine serum at 37°C, 5% CO_2. Cells subcultured every 3-4 days were transfected with linear polyethyleneimine (25 kDa, Polysciences) using the reverse transfection method according to the manufacturer's instructions. For FRET and luminescence measurements the cells were examined 24 or 48 h after transfection.

DULIP assay

HEK293 cells were reversely transfected in 96 well microtiter plates at a density of $3.75x10^4$ cells per well. 48 h after transfection cells were lysed in 100 µl HEPES lysis buffer (50 mM HEPES, 150 mM NaCl, 10% glycerol, 1% NP-40, 0.5% Deoxycholate, 20 mM NaF, 1.5 mM $MgCl_2$, 1 mM EDTA, 1 mM DTT, 1 U Benzonase, protease inhibitor cocktail (Roche, EDTA free), 1 mM PMSF) for 30 min at 4°C. Production of PA-RL- and FL-tagged fusion proteins was monitored by measuring the respective luciferase activities in crude cell lysates in 384-well microtiter plates. 10 µl of the cell lysate were added to 20 µl PBS and 10 min after the addition of 10 µl Dual-Glo® luciferase reagent (Promega) the firefly activity (FL_{IN}) was measured using an Infinite® M1000 (Tecan) plate reader. To stop the firefly luciferase activity and to measure the *Renilla* luciferase activity (RL_{IN}), 10 µl of the Dual-Glo® Stop & Glow® reagent (Promega) were added and after 15 min of incubation the activity was measured. In parallel, 50 µl of the cell lysate were incubated for 3 hours at 4°C in IgG

pre-coated 384-well microtiter plates. Plates were coated with sheep gamma globulin (Dianoca), blocked with 1% BSA in carbonate buffer (70 mM $NaHCO_3$, 30 mM Na_2CO_3, pH 9.6) before they were incubated with rabbit anti-sheep IgGs (Dianova) overnight. After cell lysate incubation, all wells were washed three times with HEPES lysis buffer before 30 µl of PBS were added to each well. Measurement of firefly (FL_{OUT}) and *Renilla* (RL_{OUT}) luminescence activity was performed using an Infinite® M1000 (Tecan) plate reader.

DULIP data analysis

To identify weakly expressing preys and weakly immunoprecipitated baits, the measured firefly or *Renilla* luciferase activities were log_2-transformed and the distribution of measured luminescence values for the controls 1 or 2 (Fig. 2d) was binned. As the expression and immunoprecipitation profiles followed Gaussian distributions, we used a Gaussian curve fit to determine the mean (µ) and standard deviation (σ) of the firefly and *Renilla* luciferase activities. Preys were classified as not expressed when the mean luminescence of the three technical replicates was smaller µ-3σ. Similarly, bait immunoprecipitation efficiency was analyzed and proteins were classified as not immunoprecipitated when the mean luminescence of the three technical replicates was smaller µ-3σ. To exclude unspecific background binding of prey proteins to antibodies or assay plates, FL_{OUT} values of PPIs of interest were divided by FL_{OUT} values of control PPIs (control 1 and 2, see Fig. 2a and Fig. S1). This revealed luminescence-based interaction control ratios (ICRs) for each PPI of interest, which were used for quality assessment of PPI detection experiments. In systematic interaction detection studies only PPIs of interest with ICRs ≥ 3 were further analyzed and the luciferase immunoprecipitation ratios (LIRs) of control 3 (see Fig. 2a) were used to calculate the normalized immunoprecipitation

ratios (NIRs) of PPIs of interest. The NIR is a measure for the success of prey protein co-immunoprecipitation in relation to the success of bait protein immunoprecipitation. Finally, to correct for unspecific background binding, we calculated the background corrected NIRs (cNIRs). The NIR value obtained for control 1 or 2 was subtracted from the calculated NIR of the interaction of interest (see also Fig. 2a and Fig. S1).

Positive and negative reference set creation

The MDC positive reference set (PRS) was generated from literature known PPIs using the HIPPIE (Human Integrated Protein-Protein Interaction rEference) database[37]. HIPPIE provides a scoring algorithm that allows a distinction between higher and lower confidence literature PPIs. For the creation of a positive reference set 25 high confidence PPIs with a HIPPIE score of ≥0.99 were chosen, of which 23 were finally tested in DULIP assays. To compile a negative reference set (NRS) the Negatome database (v1.0) was searched for PPIs that were not detected with at least 3 independent methods[38]. The cDNAs encoding 30 protein pairs were randomly selected and shuttled successfully into DULIP destination plasmids. The CCSB reference sets hsPRS-v1 and hsRRS-v1 were previously described[39].

Creating an affinity-based interaction reference set (AIRS)

The affinity-based reference set (AIRS) was generated from literature PPIs with known dissociation constants using PDBbind[40] and the Protein-Protein Interaction Affinity Database 2.0[41]. From PDBbind 47 PPIs and from PPIAD 12 PPIs were selected to cover a broad range of protein binding affinities. The cDNAs encoding 57 selected PPIs were shuttled into expression plasmids and tested in DULIP assays.

FRET measurements

HEK293 cells were reversely transfected in 96-well microtiter plates at a density of 6×10^4 cells per well. 24 h after transfection cells were fixed with 4% paraformaldehyde in PBS and washed twice with PBS. Fluorescence signals were detected with the Infinite® M1000 (Tecan) plate reader: donor channel [excitation (Ex)/emission (Em): 435 nm/475 nm], acceptor channel (Ex/Em: 500 nm/530 nm) and FRET channel (Ex/Em: 435nm/530 nm). For processing of raw data the fluorescence intensities obtained with empty vector transfected cells were used. Signals in the FRET channel (DA) were corrected for spectral bleed through of the donor (c_D) and acceptor cross-excitation (c_A) with samples expressing the donor or acceptor construct only. Finally, corrected signals in the FRET channel were normalized to the acceptor signals[35]. In brief, FRET efficiency (E_{Aapp}) in % was calculated as follows: $E_{Aapp} = (DA\text{-}c_D\times DD\text{-}c_A\times AA)/AA$ with DD = donor channel signal and AA = acceptor channel signal.

Yeast-two hybrid

The Y2H interaction mating assays were performed as previously described[3; 16]. Briefly, bait and prey constructs were transformed into yeast strains L40ccua (MATa) and L40ccα (MATα), respectively. For interaction mating, 100 µl cultures of MATa yeast strains were transferred into 96-well microtiter plates and mixed with 100 µl cultures of MATα yeast strains. The yeast mixtures were then spotted onto YPD agar plates using a spotting robot (KBiosystem). After mating for 48 h at 30°C, the yeast colonies were automatically picked and transferred into 96-well microtiter plates containing selective liquid medium (SDII-Leu-Trp). Finally, for selection of PPIs diploid yeasts were spotted in parallel onto SDIV (-Leu-Trp-Ura-His) and SDII (-Leu-

Trp) selective agar plates. After 5-6 days of incubation at 30°C agar plates were imaged and yeast growth assessed by visual inspection.

ACKNOWLEDGEMENTS

We thank Sigrid Schnoegl for critical reading of the manuscript. This work was supported by grants from the DFG (http://www.dfg.de; SFB740), the BMBF (http://www.bmbf.de; NGFN-Plus, NeuroNet, MooDS, Integrament), the EU (http://europa.eu/index_de.htm; EuroSpin and SynSys), and the Helmholtz Association (http://www.helmholtz.de; MSBN and HelMA) to EEW. The relevant grant numbers are SFB740: 740/2-11, NeuroNet: 01GS08169-73, MooDS: 01GS08150, Mutanom: 01GS08108, EuroSpin: Health-F2-2009-241498, SynSys: HEALTH-F2-2009-242167 and HelMA: HA-215. The funders had no role in the study design, the collection and analysis of data or the preparation of the manuscript.

REFERENCES

1. ***Stelzl, U. & Wanker, E. E. (2006). The value of high quality protein-protein interaction networks for systems biology. Curr Opin Chem Biol 10, 551-8.***
2. ***Braun, P. (2012). Interactome mapping for analysis of complex phenotypes: insights from benchmarking binary interaction assays. Proteomics 12, 1499-518.***
3. ***Goehler, H., Lalowski, M., Stelzl, U., Waelter, S., Stroedicke, M., Worm, U., Droege, A., Lindenberg, K. S., Knoblich, M., Haenig, C., Herbst, M., Suopanki, J., Scherzinger, E., Abraham, C., Bauer, B., Hasenbank, R., Fritzsche, A., Ludewig, A. H., Bussow, K., Coleman, S. H., Gutekunst, C. A., Landwehrmeyer, B. G., Lehrach, H. & Wanker, E. E. (2004). A protein interaction network links GIT1, an enhancer of huntingtin aggregation, to Huntington's disease. Mol Cell 15, 853-65.***
4. ***Ideker, T. & Sharan, R. (2008). Protein networks in disease. Genome Res 18, 644-52.***
5. ***Shirasaki, D. I., Greiner, E. R., Al-Ramahi, I., Gray, M., Boontheung, P., Geschwind, D. H., Botas, J., Coppola, G., Horvath, S., Loo, J. A. & Yang, X. W. (2012). Network organization of the huntingtin proteomic interactome in mammalian brain. Neuron 75, 41-57.***

6. *Menche, J., Sharma, A., Kitsak, M., Ghiassian, S. D., Vidal, M., Loscalzo, J. & Barabasi, A. L. (2015). Disease networks. Uncovering disease-disease relationships through the incomplete interactome. Science 347, 1257601.*
7. *Fields, S. & Song, O. (1989). A novel genetic system to detect protein-protein interactions. Nature 340, 245-6.*
8. *Braun, P., Tasan, M., Dreze, M., Barrios-Rodiles, M., Lemmens, I., Yu, H., Sahalie, J. M., Murray, R. R., Roncari, L., de Smet, A. S., Venkatesan, K., Rual, J. F., Vandenhaute, J., Cusick, M. E., Pawson, T., Hill, D. E., Tavernier, J., Wrana, J. L., Roth, F. P. & Vidal, M. (2009). An experimentally derived confidence score for binary protein-protein interactions. Nat Methods 6, 91-7.*
9. *Uetz, P., Giot, L., Cagney, G., Mansfield, T. A., Judson, R. S., Knight, J. R., Lockshon, D., Narayan, V., Srinivasan, M., Pochart, P., Qureshi-Emili, A., Li, Y., Godwin, B., Conover, D., Kalbfleisch, T., Vijayadamodar, G., Yang, M., Johnston, M., Fields, S. & Rothberg, J. M. (2000). A comprehensive analysis of protein-protein interactions in Saccharomyces cerevisiae. Nature 403, 623-7.*
10. *Li, S., Armstrong, C. M., Bertin, N., Ge, H., Milstein, S., Boxem, M., Vidalain, P. O., Han, J. D., Chesneau, A., Hao, T., Goldberg, D. S., Li, N., Martinez, M., Rual, J. F., Lamesch, P., Xu, L., Tewari, M., Wong, S. L., Zhang, L. V., Berriz, G. F., Jacotot, L., Vaglio, P., Reboul, J., Hirozane-Kishikawa, T., Li, Q., Gabel, H. W., Elewa, A., Baumgartner, B., Rose, D. J., Yu, H., Bosak, S., Sequerra, R., Fraser, A., Mango, S. E., Saxton, W. M., Strome, S., Van Den Heuvel, S., Piano, F., Vandenhaute, J., Sardet, C., Gerstein, M., Doucette-Stamm, L., Gunsalus, K. C., Harper, J. W., Cusick, M. E., Roth, F. P., Hill, D. E. & Vidal, M. (2004). A map of the interactome network of the metazoan C. elegans. Science 303, 540-3.*
11. *Yu, H., Braun, P., Yildirim, M. A., Lemmens, I., Venkatesan, K., Sahalie, J., Hirozane-Kishikawa, T., Gebreab, F., Li, N., Simonis, N., Hao, T., Rual, J. F., Dricot, A., Vazquez, A., Murray, R. R., Simon, C., Tardivo, L., Tam, S., Svrzikapa, N., Fan, C., de Smet, A. S., Motyl, A., Hudson, M. E., Park, J., Xin, X., Cusick, M. E., Moore, T., Boone, C., Snyder, M., Roth, F. P., Barabasi, A. L., Tavernier, J., Hill, D. E. & Vidal, M. (2008). High-quality binary protein interaction map of the yeast interactome network. Science 322, 104-10.*
12. *Vinayagam, A., Stelzl, U., Foulle, R., Plassmann, S., Zenkner, M., Timm, J., Assmus, H. E., Andrade-Navarro, M. A. & Wanker, E. E. (2011). A directed protein interaction network for investigating intracellular signal transduction. Sci Signal 4, rs8.*
13. *Weimann, M., Grossmann, A., Woodsmith, J., Ozkan, Z., Birth, P., Meierhofer, D., Benlasfer, N., Valovka, T., Timmermann, B., Wanker, E. E., Sauer, S. & Stelzl, U. (2013). A Y2H-seq approach defines the human protein methyltransferase interactome. Nat Methods 10, 339-42.*
14. *Snider, J., Hanif, A., Lee, M. E., Jin, K., Yu, A. R., Graham, C., Chuk, M., Damjanovic, D., Wierzbicka, M., Tang, P., Balderes, D., Wong, V., Jessulat, M., Darowski, K. D., San Luis, B. J., Shevelev, I., Sturley, S. L., Boone, C., Greenblatt, J. F., Zhang, Z., Paumi, C. M., Babu, M., Park, H. O., Michaelis, S. & Stagljar, I. (2013). Mapping the functional yeast ABC transporter interactome. Nat Chem Biol 9, 565-72.*

15. *Rajagopala, S. V., Sikorski, P., Kumar, A., Mosca, R., Vlasblom, J., Arnold, R., Franca-Koh, J., Pakala, S. B., Phanse, S., Ceol, A., Hauser, R., Siszler, G., Wuchty, S., Emili, A., Babu, M., Aloy, P., Pieper, R. & Uetz, P. (2014). The binary protein-protein interaction landscape of Escherichia coli. Nat Biotechnol 32, 285-90.*
16. *Stelzl, U., Worm, U., Lalowski, M., Haenig, C., Brembeck, F. H., Goehler, H., Stroedicke, M., Zenkner, M., Schoenherr, A., Koeppen, S., Timm, J., Mintzlaff, S., Abraham, C., Bock, N., Kietzmann, S., Goedde, A., Toksoz, E., Droege, A., Krobitsch, S., Korn, B., Birchmeier, W., Lehrach, H. & Wanker, E. E. (2005). A human protein-protein interaction network: a resource for annotating the proteome. Cell 122, 957-68.*
17. *Rual, J. F., Venkatesan, K., Hao, T., Hirozane-Kishikawa, T., Dricot, A., Li, N., Berriz, G. F., Gibbons, F. D., Dreze, M., Ayivi-Guedehoussou, N., Klitgord, N., Simon, C., Boxem, M., Milstein, S., Rosenberg, J., Goldberg, D. S., Zhang, L. V., Wong, S. L., Franklin, G., Li, S., Albala, J. S., Lim, J., Fraughton, C., Llamosas, E., Cevik, S., Bex, C., Lamesch, P., Sikorski, R. S., Vandenhaute, J., Zoghbi, H. Y., Smolyar, A., Bosak, S., Sequerra, R., Doucette-Stamm, L., Cusick, M. E., Hill, D. E., Roth, F. P. & Vidal, M. (2005). Towards a proteome-scale map of the human protein-protein interaction network. Nature 437, 1173-8.*
18. *Rolland, T., Tasan, M., Charloteaux, B., Pevzner, S. J., Zhong, Q., Sahni, N., Yi, S., Lemmens, I., Fontanillo, C., Mosca, R., Kamburov, A., Ghiassian, S. D., Yang, X., Ghamsari, L., Balcha, D., Begg, B. E., Braun, P., Brehme, M., Broly, M. P., Carvunis, A. R., Convery-Zupan, D., Corominas, R., Coulombe-Huntington, J., Dann, E., Dreze, M., Dricot, A., Fan, C., Franzosa, E., Gebreab, F., Gutierrez, B. J., Hardy, M. F., Jin, M., Kang, S., Kiros, R., Lin, G. N., Luck, K., MacWilliams, A., Menche, J., Murray, R. R., Palagi, A., Poulin, M. M., Rambout, X., Rasla, J., Reichert, P., Romero, V., Ruyssinck, E., Sahalie, J. M., Scholz, A., Shah, A. A., Sharma, A., Shen, Y., Spirohn, K., Tam, S., Tejeda, A. O., Trigg, S. A., Twizere, J. C., Vega, K., Walsh, J., Cusick, M. E., Xia, Y., Barabasi, A. L., Iakoucheva, L. M., Aloy, P., De Las Rivas, J., Tavernier, J., Calderwood, M. A., Hill, D. E., Hao, T., Roth, F. P. & Vidal, M. (2014). A proteome-scale map of the human interactome network. Cell 159, 1212-26.*
19. *Bruckner, A., Polge, C., Lentze, N., Auerbach, D. & Schlattner, U. (2009). Yeast two-hybrid, a powerful tool for systems biology. Int J Mol Sci 10, 2763-88.*
20. *Lievens, S., Gerlo, S., Lemmens, I., De Clercq, D. J., Risseeuw, M. D., Vanderroost, N., De Smet, A. S., Ruyssinck, E., Chevet, E., Van Calenbergh, S. & Tavernier, J. (2014). Kinase Substrate Sensor (KISS), a mammalian in situ protein interaction sensor. Mol Cell Proteomics 13, 3332-42.*
21. *Jain, A., Liu, R., Ramani, B., Arauz, E., Ishitsuka, Y., Ragunathan, K., Park, J., Chen, J., Xiang, Y. K. & Ha, T. (2011). Probing cellular protein complexes using single-molecule pull-down. Nature 473, 484-8.*
22. *Jain, A., Liu, R., Xiang, Y. K. & Ha, T. (2012). Single-molecule pull-down for studying protein interactions. Nat Protoc 7, 445-52.*
23. *Petschnigg, J., Groisman, B., Kotlyar, M., Taipale, M., Zheng, Y., Kurat, C. F., Sayad, A., Sierra, J. R., Mattiazzi Usaj, M., Snider, J., Nachman, A., Krykbaeva, I., Tsao, M. S., Moffat, J., Pawson, T., Lindquist, S., Jurisica, I. & Stagljar, I. (2014). The mammalian-membrane two-hybrid assay*

(MaMTH) for probing membrane-protein interactions in human cells. Nat Methods 11, 585-92.

24. *Barrios-Rodiles, M., Brown, K. R., Ozdamar, B., Bose, R., Liu, Z., Donovan, R. S., Shinjo, F., Liu, Y., Dembowy, J., Taylor, I. W., Luga, V., Przulj, N., Robinson, M., Suzuki, H., Hayashizaki, Y., Jurisica, I. & Wrana, J. L. (2005). High-throughput mapping of a dynamic signaling network in mammalian cells. Science 307, 1621-5.*
25. *Miller, B. W., Lau, G., Grouios, C., Mollica, E., Barrios-Rodiles, M., Liu, Y., Datti, A., Morris, Q., Wrana, J. L. & Attisano, L. (2009). Application of an integrated physical and functional screening approach to identify inhibitors of the Wnt pathway. Mol Syst Biol 5, 315.*
26. *Jia, S., Peng, J., Gao, B., Chen, Z., Zhou, Y., Fu, Q., Wang, H. & Zhan, L. (2011). Relative quantification of protein-protein interactions using a dual luciferase reporter pull-down assay system. PLoS One 6, e26414.*
27. *Petrakis, S., Rasko, T., Russ, J., Friedrich, R. P., Stroedicke, M., Riechers, S. P., Muehlenberg, K., Moller, A., Reinhardt, A., Vinayagam, A., Schaefer, M. H., Boutros, M., Tricoire, H., Andrade-Navarro, M. A. & Wanker, E. E. (2012). Identification of human proteins that modify misfolding and proteotoxicity of pathogenic ataxin-1. PLoS Genet 8, e1002897.*
28. *Taipale, M., Krykbaeva, I., Koeva, M., Kayatekin, C., Westover, K. D., Karras, G. I. & Lindquist, S. (2012). Quantitative analysis of HSP90-client interactions reveals principles of substrate recognition. Cell 150, 987-1001.*
29. *Fossati, G., Morini, R., Corradini, I., Antonucci, F., Trepte, P., Edry, E., Sharma, V., Papale, A., Pozzi, D., Defilippi, P., Meier, J. C., Brambilla, R., Turco, E., Rosenblum, K., Wanker, E. E., Ziv, N. E., Menna, E. & Matteoli, M. (2015). Reduced SNAP-25 increases PSD-95 mobility and impairs spine morphogenesis. Cell Death Differ.*
30. *Xu, G., Barrios-Rodiles, M., Jerkic, M., Turinsky, A. L., Nadon, R., Vera, S., Voulgaraki, D., Wrana, J. L., Toporsian, M. & Letarte, M. (2014). Novel protein interactions with endoglin and activin receptor-like kinase 1: potential role in vascular networks. Mol Cell Proteomics 13, 489-502.*
31. *Taipale, M., Tucker, G., Peng, J., Krykbaeva, I., Lin, Z. Y., Larsen, B., Choi, H., Berger, B., Gingras, A. C. & Lindquist, S. (2014). A quantitative chaperone interaction network reveals the architecture of cellular protein homeostasis pathways. Cell 158, 434-48.*
32. *Ottilie, S., Diaz, J. L., Horne, W., Chang, J., Wang, Y., Wilson, G., Chang, S., Weeks, S., Fritz, L. C. & Oltersdorf, T. (1997). Dimerization properties of human BAD. Identification of a BH-3 domain and analysis of its binding to mutant BCL-2 and BCL-XL proteins. J Biol Chem 272, 30866-72.*
33. *Zha, J., Harada, H., Osipov, K., Jockel, J., Waksman, G. & Korsmeyer, S. J. (1997). BH3 domain of BAD is required for heterodimerization with BCL-XL and pro-apoptotic activity. J Biol Chem 272, 24101-4.*
34. *Blasche, S. & Koegl, M. (2013). Analysis of protein-protein interactions using LUMIER assays. Methods Mol Biol 1064, 17-27.*
35. *Jiang, X. & Sorkin, A. (2002). Coordinated traffic of Grb2 and Ras during epidermal growth factor receptor endocytosis visualized in living cells. Mol Biol Cell 13, 1522-35.*

36. *Buntru, A., Zimmermann, T. & Hauck, C. R. (2009). Fluorescence resonance energy transfer (FRET)-based subcellular visualization of pathogen-induced host receptor signaling. BMC Biol 7, 81.*
37. *Schaefer, M. H., Fontaine, J. F., Vinayagam, A., Porras, P., Wanker, E. E. & Andrade-Navarro, M. A. (2012). HIPPIE: Integrating protein interaction networks with experiment based quality scores. PLoS One 7, e31826.*
38. *Smialowski, P., Pagel, P., Wong, P., Brauner, B., Dunger, I., Fobo, G., Frishman, G., Montrone, C., Rattei, T., Frishman, D. & Ruepp, A. (2010). The Negatome database: a reference set of non-interacting protein pairs. Nucleic Acids Res 38, D540-4.*
39. *Venkatesan, K., Rual, J. F., Vazquez, A., Stelzl, U., Lemmens, I., Hirozane-Kishikawa, T., Hao, T., Zenkner, M., Xin, X., Goh, K. I., Yildirim, M. A., Simonis, N., Heinzmann, K., Gebreab, F., Sahalie, J. M., Cevik, S., Simon, C., de Smet, A. S., Dann, E., Smolyar, A., Vinayagam, A., Yu, H., Szeto, D., Borick, H., Dricot, A., Klitgord, N., Murray, R. R., Lin, C., Lalowski, M., Timm, J., Rau, K., Boone, C., Braun, P., Cusick, M. E., Roth, F. P., Hill, D. E., Tavernier, J., Wanker, E. E., Barabasi, A. L. & Vidal, M. (2009). An empirical framework for binary interactome mapping. Nat Methods 6, 83-90.*
40. *Wang, R., Fang, X., Lu, Y. & Wang, S. (2004). The PDBbind database: collection of binding affinities for protein-ligand complexes with known three-dimensional structures. J Med Chem 47, 2977-80.*
41. *Kastritis, P. L., Moal, I. H., Hwang, H., Weng, Z., Bates, P. A., Bonvin, A. M. & Janin, J. (2011). A structure-based benchmark for protein-protein binding affinity. Protein Sci 20, 482-91.*
42. *Landgraf, C., Panni, S., Montecchi-Palazzi, L., Castagnoli, L., Schneider-Mergener, J., Volkmer-Engert, R. & Cesareni, G. (2004). Protein interaction networks by proteome peptide scanning. PLoS Biol 2, E14.*
43. *Wang, X., Wei, X., Thijssen, B., Das, J., Lipkin, S. M. & Yu, H. (2012). Three-dimensional reconstruction of protein networks provides insight into human genetic disease. Nat Biotechnol 30, 159-64.*
44. *Hata, Y., Slaughter, C. A. & Sudhof, T. C. (1993). Synaptic vesicle fusion complex contains unc-18 homologue bound to syntaxin. Nature 366, 347-51.*
45. *Han, G. A., Malintan, N. T., Saw, N. M., Li, L., Han, L., Meunier, F. A., Collins, B. M. & Sugita, S. (2011). Munc18-1 domain-1 controls vesicle docking and secretion by interacting with syntaxin-1 and chaperoning it to the plasma membrane. Mol Biol Cell 22, 4134-49.*
46. *Meijer, M., Burkhardt, P., de Wit, H., Toonen, R. F., Fasshauer, D. & Verhage, M. (2012). Munc18-1 mutations that strongly impair SNARE-complex binding support normal synaptic transmission. EMBO J 31, 2156-68.*
47. *Ellis, J. D., Barrios-Rodiles, M., Colak, R., Irimia, M., Kim, T., Calarco, J. A., Wang, X., Pan, Q., O'Hanlon, D., Kim, P. M., Wrana, J. L. & Blencowe, B. J. (2012). Tissue-specific alternative splicing remodels protein-protein interaction networks. Mol Cell 46, 884-92.*
48. *Rhee HW, Z. P., Udeshi ND, Martell JD, Mootha VK, Carr SA, Ting AY. (2013). Proteomic mapping of mitochondria in living cells via spatially restricted enzymatic tagging. Science 339, 1328-31.*

49. Schluter, K., Schleicher, M. & Jockusch, B. M. (1998). Effects of single amino acid substitutions in the actin-binding site on the biological activity of bovine profilin I. J Cell Sci 111 (Pt 22), 3261-73.

50. Palidwor, G. A., Shcherbinin, S., Huska, M. R., Rasko, T., Stelzl, U., Arumughan, A., Foulle, R., Porras, P., Sanchez-Pulido, L., Wanker, E. E. & Andrade-Navarro, M. A. (2009). Detection of alpha-rod protein repeats using a neural network and application to huntingtin. PLoS Comput Biol 5, e1000304.

FIGURE LEGENDS

Fig. 1: DULIP vectors and proteins utilized for PPI testing.

(**a**) Scheme of Gateway compatible plasmids for expression of bait and prey hybrid proteins. AttR sites flank the gateway cassette (GW) and allow the introduction of open-reading frames via LR recombination reaction. Bait vectors enable the expression of N- or C-terminally tagged RL fusions harboring also a protein A (PA) tag. The PA tag facilitates the efficient immunoprecipitation of bait proteins. Prey vectors encode N- or C-terminally tagged FL fusion proteins. The prey proteins additionally harbor a V5 epitope tag for their detection on immunoblots. RL: *Renilla* luciferase; FL: firefly luciferase; PA: Protein A; V5: V5-tag; Amp: ampicillin resistance; Neo: neomycin resistance; Cam: chloramphenicol resistance; ccdB: ccdB gene; AttR1/AttR2: Gateway® recombination sites; GW: Gateway® cassette. (**b**) Schematic depiction of hybrid fusion proteins utilized to study the published interaction between BAD and BCL2L1 with DULIP assays.

Fig. 2: Investigating the interaction between BAD and BCL2L1 with DULIP assays.

(**a**) Schematic representation of the DULIP approach. To assess the interaction between the proteins BAD (bait) and BCL2L1 (prey) the fusion proteins PA-RL-BAD/FL-BCL2L1 (PPI), PA-RL-BAD/FL-mCherry (Control 1) and PA-RL-mCherry/ FL-BCL2L1 (Control 2) were co-produced in HEK293 cells. In addition, cells were analyzed expressing the fusion protein PA-RL-FL (Control 3). (**b**) Analysis of protein expression through quantification of RL and FL luminescence activities in cell lysates. Cell lysates were investigated 48 h post transfection (**c**) Analysis of co-immunoprecipitates through quantification of RL and FL luciferase activities. The PA-

tagged bait proteins were immunoprecipitated in IgG-coated microtiter plates. (**d**) Calculation of normalized interaction ratios (NIRs) for tested PPIs. The NIR for the interaction PA-RL-BAD/FL-BCL2L1 was significantly higher than the NIRs for the control PPIs PA-RL-BAD/FL-mCherry, PA-RL-mCherry/FL-BCL2L1. Finally, for the PPI of interest PA-RL-BAD/FL-BCL2L1 a background corrected normalized interaction ratio (cNIR) was calculated. All values are means of two independent experiments performed in triplicates each ± SEM. Two-tailed unpaired t-test; ***p<0.001.

Fig. 3: Systematic analysis of positive and negative interaction reference sets using DULIP assays.

(**a**) Selection strategy for interaction pairs compiled in the positive reference set (PRS). From 181 PPIs with a confidence score ≥ 0.99 (HIPPIE database) 25 protein pairs were randomly selected, of which 23 were examined in DULIP assays. (**b**) Selection scheme for PPIs compiled in the negative reference set (NRS). We selected 30 PPIs from the Negatome database (v1.0) for systematic interaction testing in DULIP assays. (**c**) Investigation of the reproducibility of DULIP PPI mapping experiments. cNIR values were calculated for all interactions of the PRS and the NRS. The scatter plot shows the mean cNIRs of three technical replicates from two biological replicates (expiments 1 and 2). Error bars are SEM of three technical replicates. (**d**) Estimation of assay sensitivity through receiver operating characteristic (ROC) analysis. A cNIR of ≥3 was optimal to separate positive and negative PPIs with DULIP assays. (**e**) With a benchmarked DULIP assay high-confidence human PPIs were detected with a sensitivity of 79.5% and a specificity of

96.7% in the MDC-generated reference sets. In the previously published CCSB reference sets hsPRS-v1 and hsRRS-v1 PPIs were recovered with a success rate of 34.8 and 3.7%, respectively. (**f**) and (**g**) Interactions with the higher luminescence-based interaction ratios are shown from the MDC PPI sets a and b. Values are displayed as a bar diagram (means ± SEM of two biological replicates). PPIs surpassing the cNIR threshold (dotted line) are considered positive and are colored blue. Negative PPIs are indicated by red color.

Fig. 4: Systematic analysis of interactions with known binding affinities using the DULIP assay.

(**a**) Selection strategy for interaction pairs compiled in the affinity-based interaction reference set (AIRS). We selected 57 PPIs from PDBbind and the Protein-Protein-Interaction Affinity Database 2.0 and systematically tested them in DULIP assays. (**b**) The selected 57 PPIs in the AIRS span a broad range of binding affinities. (**c**) Detection rate of PPIs with DULIP assays in relation to their published binding affinities. (**d**) Number of tested PPIs for the respective binding affinity range and numbers of interactions detected with DULIP assays. (**e**) Published dissociation constants of DULIP positive interactions plotted against luminescence-based cNIR values. Linear regression plotted as dashed line. Pearson correlation: *$p<0.05$.

Fig. 5: Point mutations influence the association between Munc18 and Syntaxin-1 in interaction detection assays.

(**a**) High resolution structure depicting the binding interface of the Syntaxin-1 (amino acids 110-121 and 222-240) and Munc18 (amino acids 30-61) protein complex (Burkhardt 2008 EMBO; PDB: 3C98). Point mutations in Munc18 that influence the

interaction strength are highlighted. (**b**) Previously published studies indicate that point mutations influence the binding affinity of the interacting proteins Munc18 and Syntaxin-1[44; 45; 46]; nd: not determined; -: no interaction detected. (**c**) Analysis of the effects of point mutations on the interaction between Munc18 and Syntaxin-1 with DULIP. For all tested protein pairs cNIRs were determined. Values are the means of two independent experiments performed in triplicates each ± SEM. The dotted line indicates the threshold (cNIR ≥3) above which positive PPIs are scored with DULIP assays. (**d**) Analysis of the effects of point mutations on the interaction between Munc18 and Syntaxin-1 with Y2H interaction assays. Representative interaction mating experiments on selective agar plates are shown. (**e**) Quantification of data from Y2H interaction mating experiments. The data from eight mating experiments with three technical replicates each were analyzed. Bars represent mean values ± SEM. Statistical significance was assessed by two-sided Fisher's exact test; ***p<0.001.

Fig. S1: Step-by-step instructions for DULIP data analysis.

Step 1: Measure Expression (IN). Transfected cells are lysed and the expression of bait and prey proteins was measured through quantification of luminescence activities. Preys with significantly weaker firefly activity (FL_{IN}) than the FL_{IN} mean signals of all control 1 preys are excluded from further data analysis.

Step 2: Measure Immunoprecipitation (OUT). Cell lysates are subjected to immunoprecipitation and the RL_{OUT} and FL_{OUT} luciferase activities in the immunoprecipitates are finally measured. Baits that are insufficiently immunoprecipitated are excluded from further data analysis if their measured RL_{OUT} activities are significantly lower than the mean RL_{OUT} signals of all Control 2 baits.

Step 3: Interaction Control Ratios (ICRs). FL_{OUT} values of PPIs of interest were divided by FL_{OUT} values of control PPIs (control 1 and 2, see Fig. 2a and Fig. S1). This revealed luminescence-based interaction control ratios (ICRs) for each PPI of interest, which were used for quality assessment of PPIs. Only PPIs of interest with ICRs ≥ 3 were further analyzed.

Step 4: Normalized Immunoprecipitation Ratios (NIRs). The normalized immunoprecipitation ratio (NIR) is determined as the relative amount of FL-X that is bound to PA-RL-Y in relation to the PA-RL-FL tandem construct (Control 3).

Step 5: Background corrected NIRs (cNIRs). The relative background binding of each tested bait or prey protein to the luciferase fused to an unrelated protein (mCherry) is determined. The protein (bait or prey) that gives the higher background is subtracted from the calculated NIR of each protein of interest. More detailed information is also provided in the materials and methods section.

Fig. S2: Investigating the interaction between BAD and BCL2L1 using Y2H and FRET assays.

(**a**) Representative interaction mating experiment. Diploid yeast strains co-expressing the proteins LexA-BAD/Gal4-BCL2L1, LexA-mCherry/ Gal4-BCL2L1 or Gal4-LexA/Gal4-mCherry were analyzed. (**b**) Quantification of yeast colony growth. 12 independent mating experiments with three technical replicates each were analyzed. Bars represent mean values ± SEM. Two-sided Fisher's exact test; ***p<0.001. (**c**) Analysis of the interaction between BAD and BCL2L1 using FRET assays. HEK293 cells were assessed 24 h post transfection using a fluorescence plate reader. FRET values for tested protein combinations were calculated using the sensitized emission

method. FRET efficiencies are the mean values of three independent experiments performed in triplicates each ± SEM (ns: non-significant, ***p<0.001).

Fig. S3: Overview of selected PPIs for DULIP benchmarking studies.

(**a**) Schematic representation of tested PPIs from the PRS and the NRS generated at the MDC. PPIs were assessed in both configurations (set a and b) in two independent experiments (Exp 1 and 2). Green color indicates PPIs that were successfully screened with DULIP assays. PPIs for which cloning failed (blue triangles), prey proteins were not expressed (yellow triangles) or bait proteins were insufficiently immunoprecipitated (red triangles) were excluded from further analysis. (**b**) Estimation of prey protein expression. FL signals (FL_{IN}) obtained for preys are presented as a frequency distribution. Data from two biological replicates (Exp 1 and 2) were log_2-transformed prior to analysis. Based on the log_2-transformed FL signals of PPIs examined in control 1 experiments (Fig. 2d), a Gaussian fit was applied to identify non-expressed prey proteins (broken lines). (**c**) Estimation of the success of bait immunoprecipitation. Bait RL signals (RL_{OUT}) from experiments 1 and 2 were log_2-transformed and presented as a frequency distribution. Based on the log_2-transformed RL signals of PPIs examined in control 2 experiments, a Gaussian fit was applied to identify bait proteins that are insufficiently immunoprecipitated (broken lines).

Fig. S4: Comparison of biological replicates of DULIP tested PPIs.

(**a**) and (**b**) Representation of PPIs from the PRS (sets a and b). Data (cNIRs) are displayed as means ± SEM from three technical replicates each for experiments 1 and 2. Positive PPIs are shown in dark (Exp 1) or light blue (Exp 2) colors. Negative

PPIs are presented in red (Exp 1 and 2) colors. (**c**) and (**d**) Representation of PPIs from the NRS; cNIRs calculated for PPIs from the sets a and b are shown using the same color code as in a and b.

Fig. S5: Systematic analysis of PPIs in hsPRS-v1 and hsRRS-v1 reference sets using DULIP assays.

(**a**) and (**b**) From 92 PPIs in the published hsPRS-v1 and hsRRS-v1 reference sets 82 PPIs were selected in each case and examined in DULIP assays. (**c**) and (**d**) Data are displayed as cNIRs for the PPI sets a and b. Values are displayed as a bar diagram (means ± SEM of two biological replicates). PPIs surpassing the cNIR threshold (dotted line) are considered positive and are colored blue. Negative PPIs are indicated by red color.

Fig. S6: Selected PPIs from the reference sets hsPRS-v1 and hsRRS-v1 for DULIP interaction studies.

(**a**) and (**b**) Schematic representation of tested PPIs from the hsPRS-v1 and the hsRRS-v1 reference sets; PPIs were examined in two configurations (sets a and b) and two independent experiments (Exp 1 and 2). Green color indicates PPIs that were successfully screened with DULIP assays. PPIs that were not cloned (blue triangles), prey proteins not expressed (yellow triangles) or bait proteins insufficiently immunoprecipitated (red triangles) were excluded from further analysis.

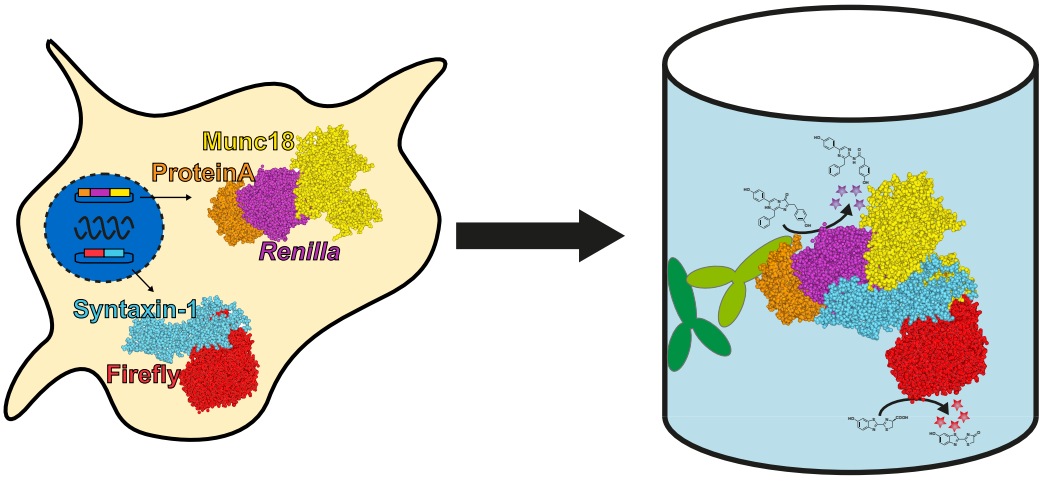

Graphical Abstract

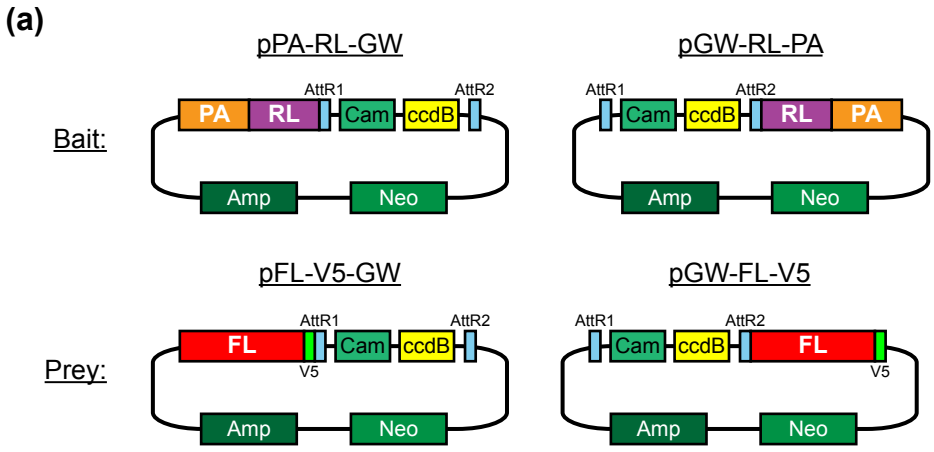
(a)
pPA-RL-GW
pGW-RL-PA
Bait:
AttR1
AttR2
PA
RL
Cam
ccdB
Amp
Neo
pFL-V5-GW
pGW-FL-V5
Prey:
FL
V5
(b)
PA-RL-FL:
PA-RL-BAD:
PA-RL-mCherry:
FL-BCL2L1:
FL-mCherry:
BAD
mCherry
BCL2L1

Figure 1

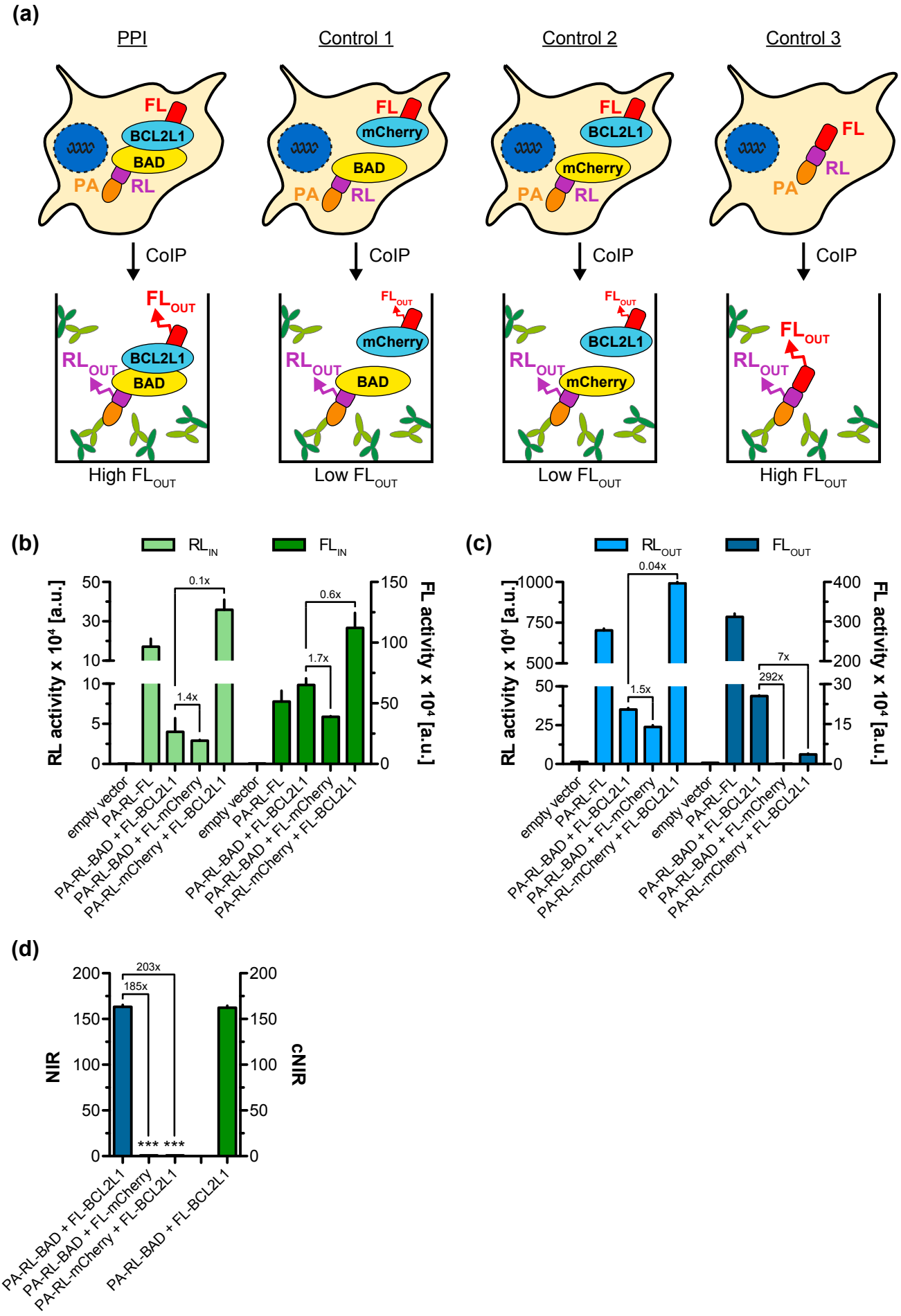
(a)
PPI
Control 1
Control 2
Control 3
FL
BCL2L1
BAD
PA
RL
mCherry
CoIP
FL_OUT
RL_OUT
High FL_OUT
Low FL_OUT
Low FL_OUT
High FL_OUT
(b)
RL_IN
FL_IN
RL activity x 10⁴ [a.u.]
FL activity x 10⁴ [a.u.]
0.1x
1.4x
0.6x
1.7x
empty vector
PA-RL-FL
PA-RL-BAD + FL-BCL2L1
PA-RL-BAD + FL-mCherry
PA-RL-mCherry + FL-BCL2L1
(c)
RL_OUT
FL_OUT
0.04x
1.5x
7x
292x
(d)
NIR
cNIR
203x
185x
*** ***
PA-RL-BAD + FL-BCL2L1
PA-RL-BAD + FL-mCherry
PA-RL-mCherry + FL-BCL2L1
PA-RL-BAD + FL-BCL2L1

Figure 2

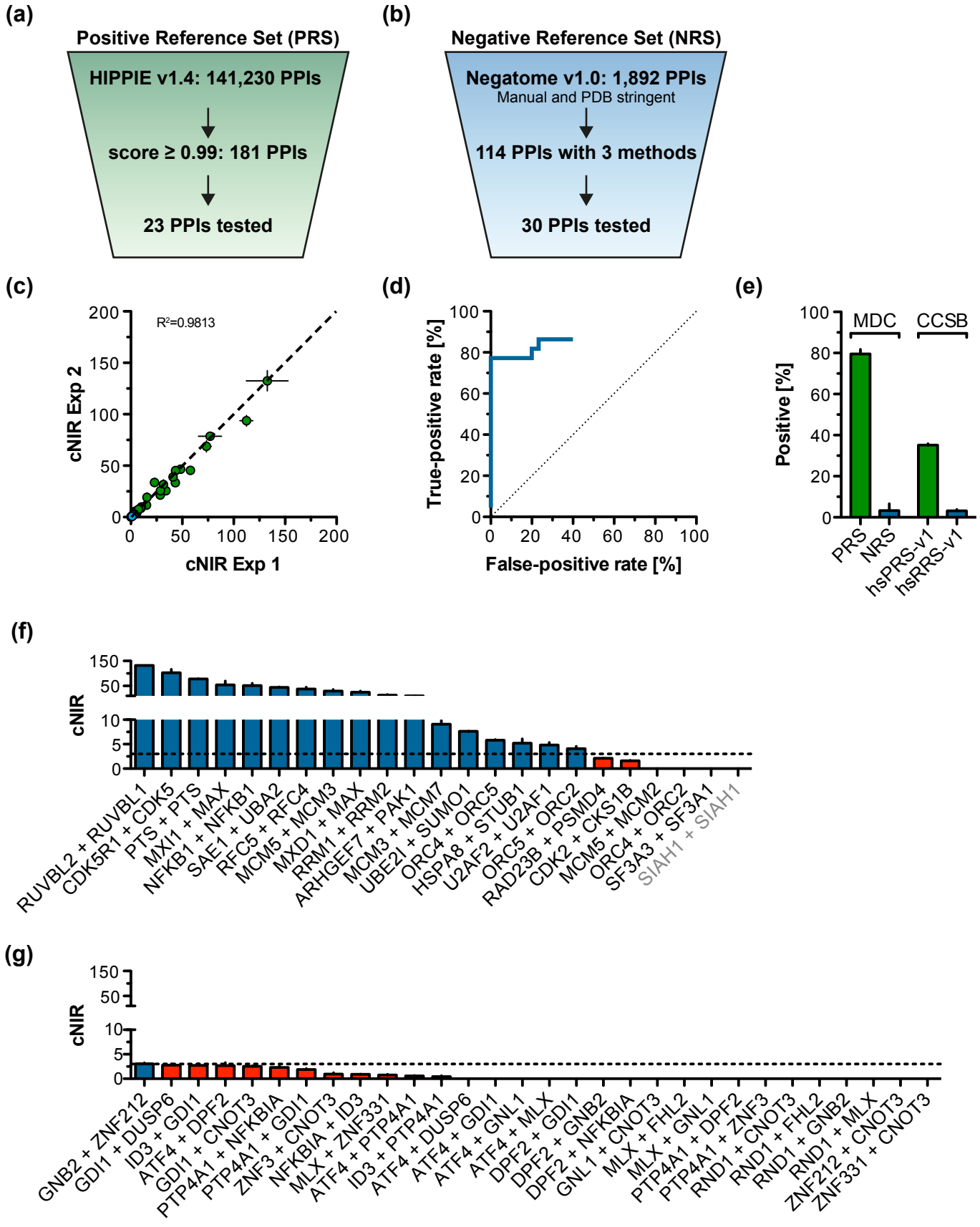
(a)
Positive Reference Set (PRS)
HIPPIE v1.4: 141,230 PPIs
score ≥ 0.99: 181 PPIs
23 PPIs tested
(b)
Negative Reference Set (NRS)
Negatome v1.0: 1,892 PPIs
Manual and PDB stringent
114 PPIs with 3 methods
30 PPIs tested
(c)
R²=0.9813
cNIR Exp 2
cNIR Exp 1
(d)
True-positive rate [%]
False-positive rate [%]
(e)
MDC
CCSB
Positive [%]
PRS
NRS
hsPRS-v1
hsRRS-v1
(f)
cNIR
RUVBL2 + RUVBL1
CDK5R1 + CDK5
PTS + PTS
MXI1 + MAX
NFKB1 + NFKB1
SAE1 + UBA2
RFC5 + RFC4
MCM5 + MCM3
MXD1 + MAX
RRM1 + RRM2
ARHGEF7 + PAK1
MCM3 + MCM7
UBE2I + SUMO1
ORC4 + ORC5
HSPA8 + STUB1
U2AF2 + U2AF1
ORC5 + ORC2
RAD23B + PSMD4
CDK2 + CKS1B
MCM5 + MCM2
ORC4 + ORC2
SF3A3 + SF3A1
SIAH1 + SIAH1
(g)
cNIR
GNB2 + ZNF212
GDI1 + DUSP6
ID3 + GDI1
ATF4 + DPF2
GDI1 + CNOT3
PTP4A1 + NFKBIA
PTP4A1 + GDI1
ZNF3 + CNOT3
NFKBIA + ID3
MLX + ZNF331
ATF4 + PTP4A1
ID3 + PTP4A1
ATF4 + DUSP6
ATF4 + GDI1
ATF4 + GNL1
ATF4 + MLX
DPF2 + GDI1
DPF2 + GNB2
DPF2 + NFKBIA
GNL1 + CNOT3
MLX + FHL2
MLX + GNL1
PTP4A1 + DPF2
PTP4A1 + ZNF3
RND1 + CNOT3
RND1 + FHL2
RND1 + GNB2
RND1 + MLX
ZNF212 + CNOT3
ZNF331 + CNOT3

Figure 3

(a)

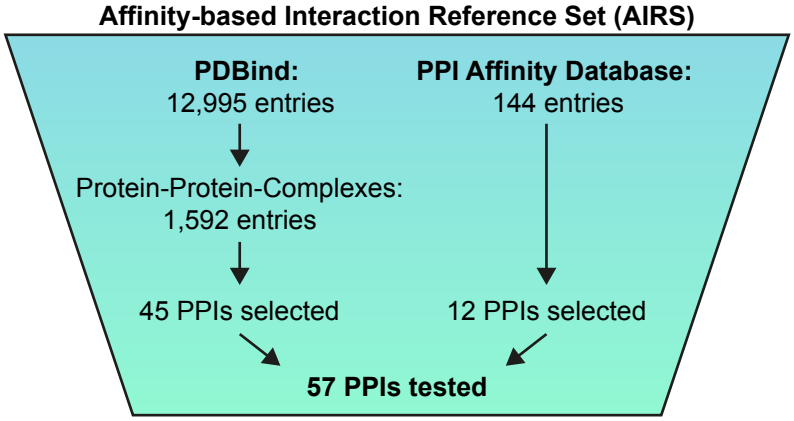

(b)

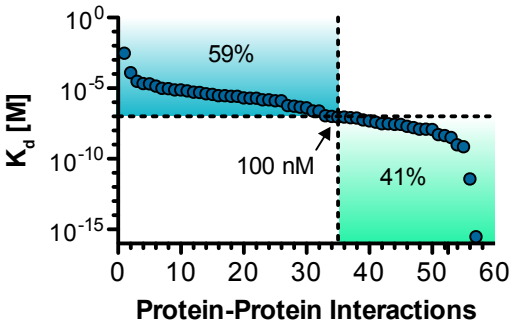

(c)

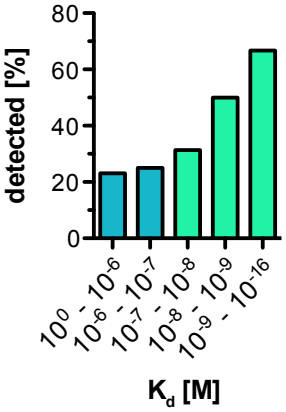

(d)

K_d [M]	tested	positive	positive
10^{0} - 10^{-6}	26	6	23.1%
10^{-6} - 10^{-7}	8	2	25.0%
10^{-7} - 10^{-8}	16	5	31.3%
10^{-8} - 10^{-9}	4	2	50.0%
10^{-9} - 10^{-16}	3	2	66.7%

(e)

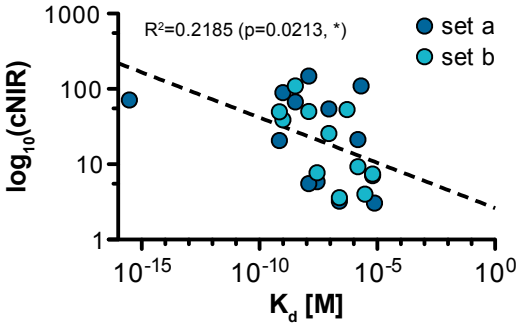

Figure 4

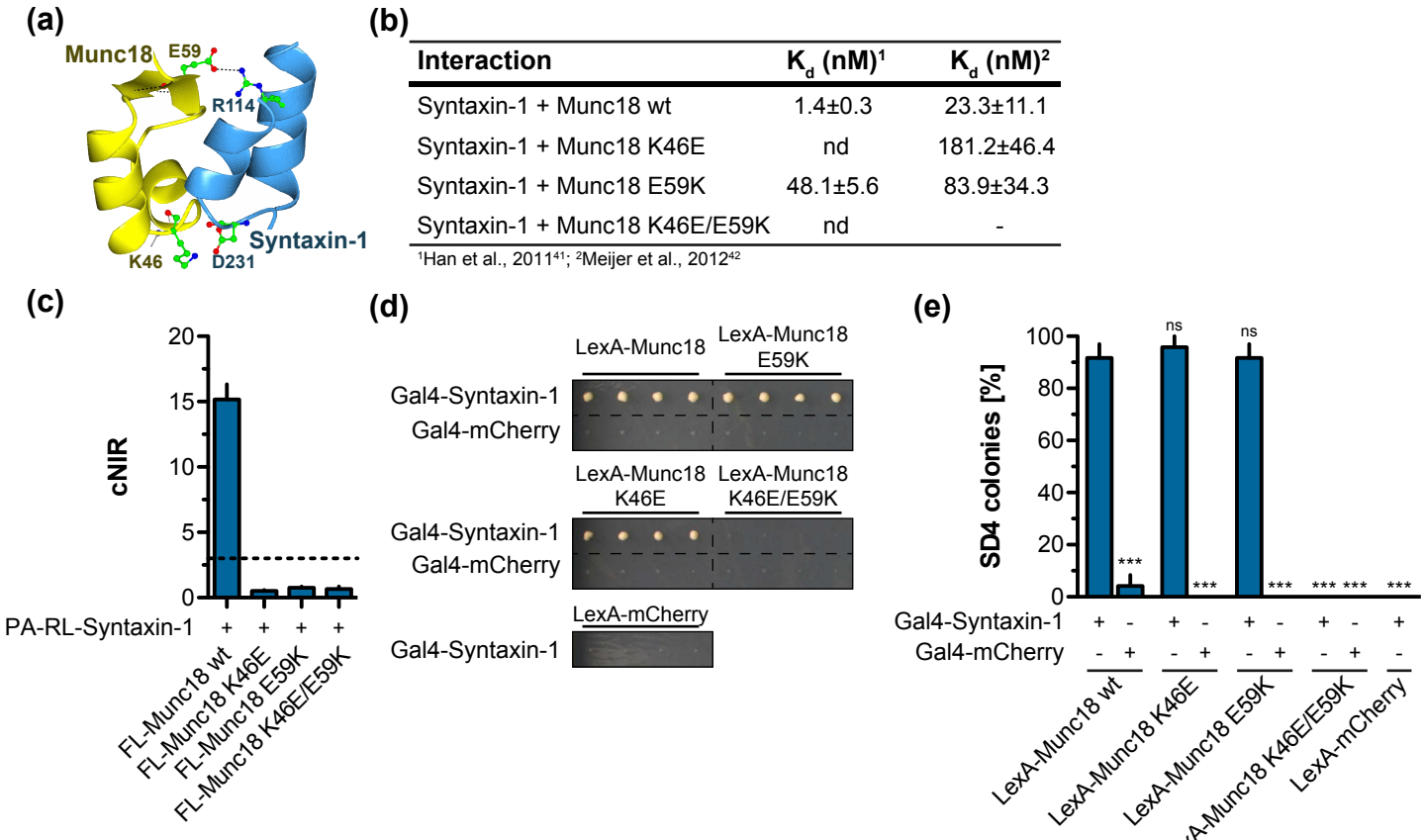
(a)
Munc18
E59
R114
Syntaxin-1
K46
D231
(b)
Interaction
Kd (nM)1
Kd (nM)2
Syntaxin-1 + Munc18 wt
1.4±0.3
23.3±11.1
Syntaxin-1 + Munc18 K46E
nd
181.2±46.4
Syntaxin-1 + Munc18 E59K
48.1±5.6
83.9±34.3
Syntaxin-1 + Munc18 K46E/E59K
nd
-
1Han et al., 2011[41]; 2Meijer et al., 2012[42]
(c)
cNIR
PA-RL-Syntaxin-1
FL-Munc18 wt
FL-Munc18 K46E
FL-Munc18 E59K
FL-Munc18 K46E/E59K
(d)
LexA-Munc18
LexA-Munc18 E59K
Gal4-Syntaxin-1
Gal4-mCherry
LexA-Munc18 K46E
LexA-Munc18 K46E/E59K
LexA-mCherry
(e)
SD4 colonies [%]
ns
Gal4-Syntaxin-1
Gal4-mCherry
LexA-Munc18 wt
LexA-Munc18 K46E
LexA-Munc18 E59K
LexA-Munc18 K46E/E59K
LexA-mCherry

Figure 5

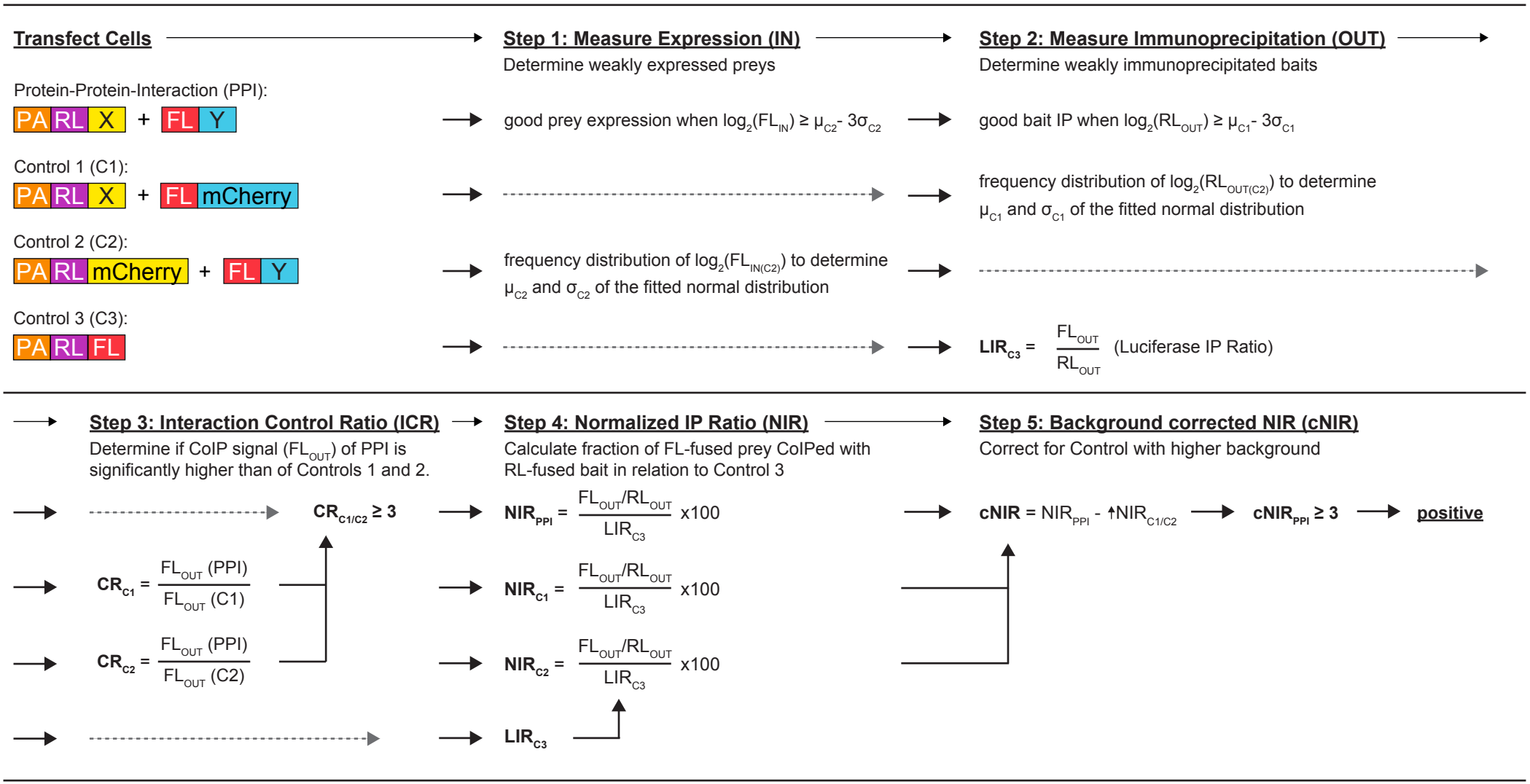
Transfect Cells
Step 1: Measure Expression (IN)
Determine weakly expressed preys
Step 2: Measure Immunoprecipitation (OUT)
Determine weakly immunoprecipitated baits
Protein-Protein-Interaction (PPI):
PA RL X + FL Y
good prey expression when log2(FLIN) ≥ μC2- 3σC2
good bait IP when log2(RLOUT) ≥ μC1- 3σC1
Control 1 (C1):
PA RL X + FL mCherry
frequency distribution of log2(RLOUT(C2)) to determine μC1 and σC1 of the fitted normal distribution
Control 2 (C2):
PA RL mCherry + FL Y
frequency distribution of log2(FLIN(C2)) to determine μC2 and σC2 of the fitted normal distribution
Control 3 (C3):
PA RL FL
LIRC3 = FLOUT / RLOUT (Luciferase IP Ratio)
Step 3: Interaction Control Ratio (ICR)
Determine if CoIP signal (FLOUT) of PPI is significantly higher than of Controls 1 and 2.
Step 4: Normalized IP Ratio (NIR)
Calculate fraction of FL-fused prey CoIPed with RL-fused bait in relation to Control 3
Step 5: Background corrected NIR (cNIR)
Correct for Control with higher background
CRC1/C2 ≥ 3
NIRPPI = (FLOUT/RLOUT) / LIRC3 x100
CRC1 = FLOUT (PPI) / FLOUT (C1)
NIRC1 = (FLOUT/RLOUT) / LIRC3 x100
CRC2 = FLOUT (PPI) / FLOUT (C2)
NIRC2 = (FLOUT/RLOUT) / LIRC3 x100
LIRC3
cNIR = NIRPPI - ↑NIRC1/C2
cNIRPPI ≥ 3
positive

Figure S1

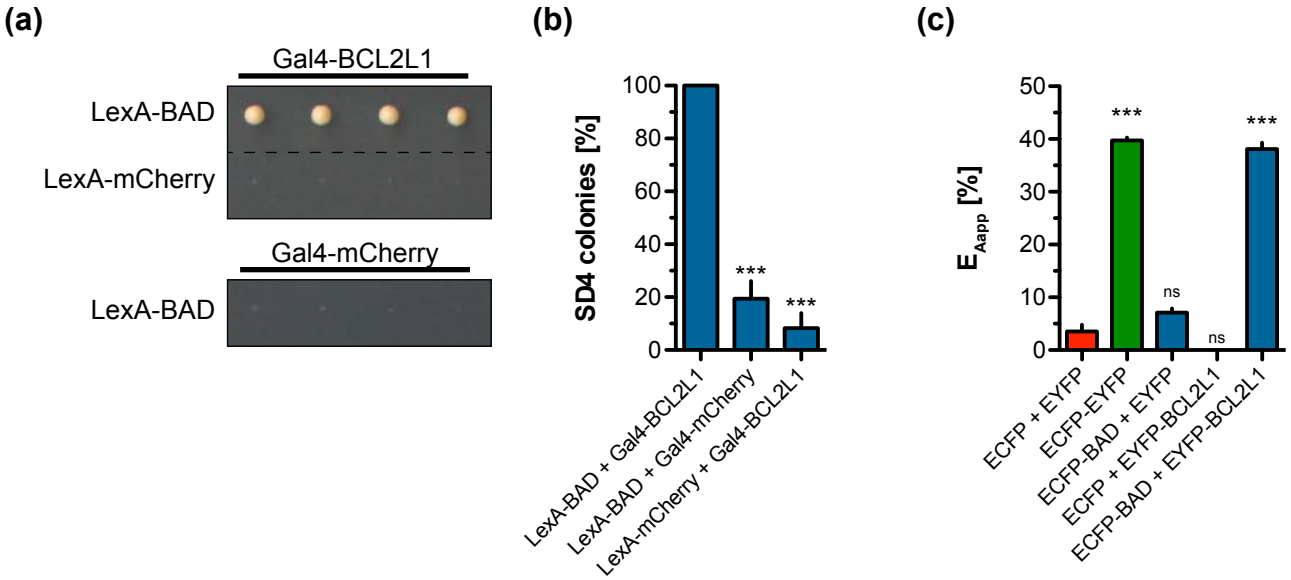
(a)
Gal4-BCL2L1
LexA-BAD
LexA-mCherry
Gal4-mCherry
LexA-BAD
(b)
SD4 colonies [%]
100
80
60
40
20
0
***
***
LexA-BAD + Gal4-BCL2L1
LexA-BAD + Gal4-mCherry
LexA-mCherry + Gal4-BCL2L1
(c)
E Aapp [%]
50
40
30
20
10
0
***
ns
ns
***
ECFP + EYFP
ECFP-EYFP
ECFP-BAD + EYFP
ECFP + EYFP-BCL2L1
ECFP-BAD + EYFP-BCL2L1

Figure S2

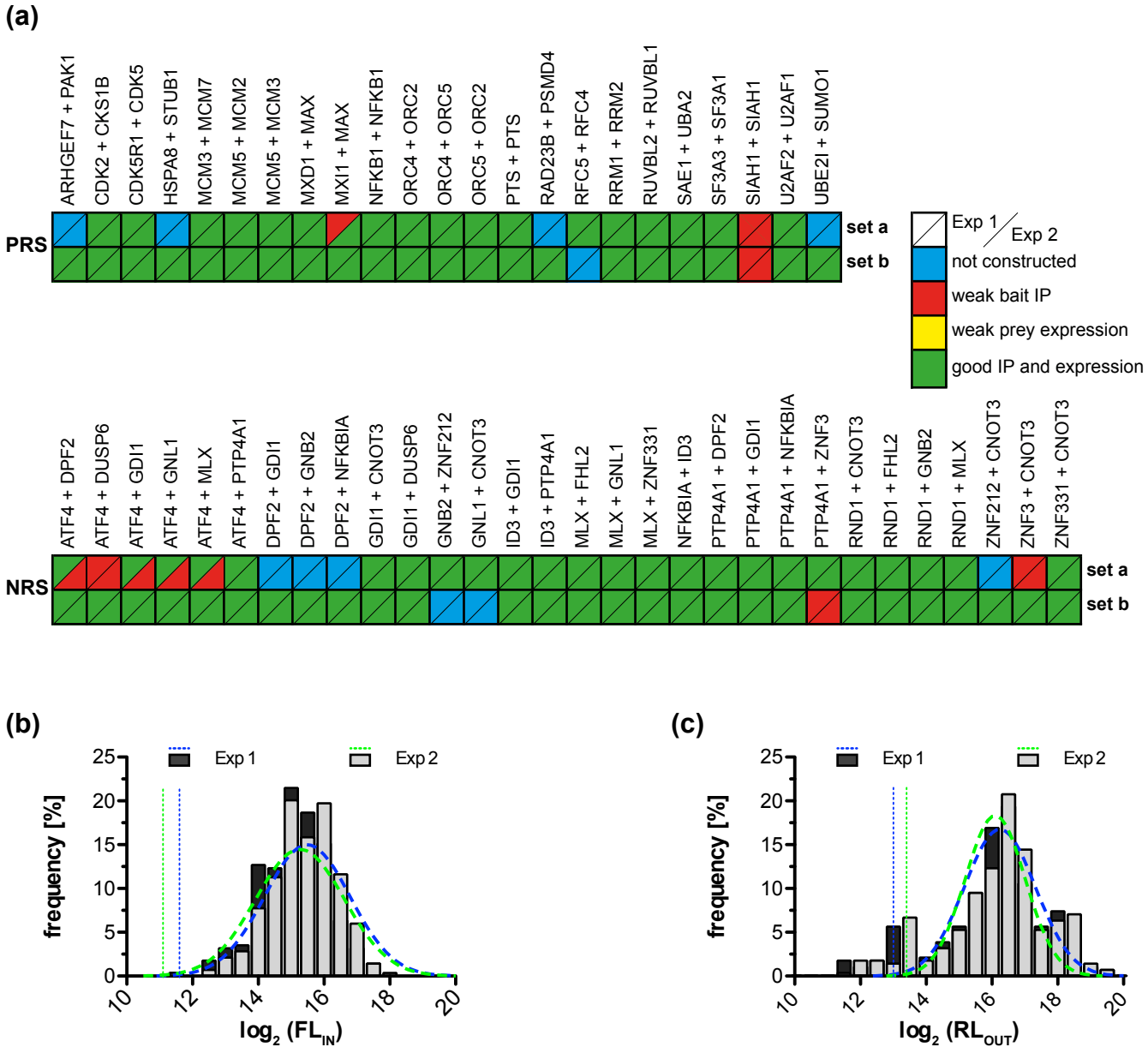
(a)
PRS
ARHGEF7 + PAK1
CDK2 + CKS1B
CDK5R1 + CDK5
HSPA8 + STUB1
MCM3 + MCM7
MCM5 + MCM2
MCM5 + MCM3
MXD1 + MAX
MXI1 + MAX
NFKB1 + NFKB1
ORC4 + ORC2
ORC4 + ORC5
ORC5 + ORC2
PTS + PTS
RAD23B + PSMD4
RFC5 + RFC4
RRM1 + RRM2
RUVBL2 + RUVBL1
SAE1 + UBA2
SF3A3 + SF3A1
SIAH1 + SIAH1
U2AF2 + U2AF1
UBE2I + SUMO1
set a
set b
Exp 1
Exp 2
not constructed
weak bait IP
weak prey expression
good IP and expression
NRS
ATF4 + DPF2
ATF4 + DUSP6
ATF4 + GDI1
ATF4 + GNL1
ATF4 + MLX
ATF4 + PTP4A1
DPF2 + GDI1
DPF2 + GNB2
DPF2 + NFKBIA
GDI1 + CNOT3
GDI1 + DUSP6
GNB2 + ZNF212
GNL1 + CNOT3
ID3 + GDI1
ID3 + PTP4A1
MLX + FHL2
MLX + GNL1
MLX + ZNF331
NFKBIA + ID3
PTP4A1 + DPF2
PTP4A1 + GDI1
PTP4A1 + NFKBIA
PTP4A1 + ZNF3
RND1 + CNOT3
RND1 + FHL2
RND1 + GNB2
RND1 + MLX
ZNF212 + CNOT3
ZNF3 + CNOT3
ZNF331 + CNOT3
set a
set b
(b)
frequency [%]
Exp 1
Exp 2
log2 (FLIN)
(c)
frequency [%]
Exp 1
Exp 2
log2 (RLOUT)

Figure S3

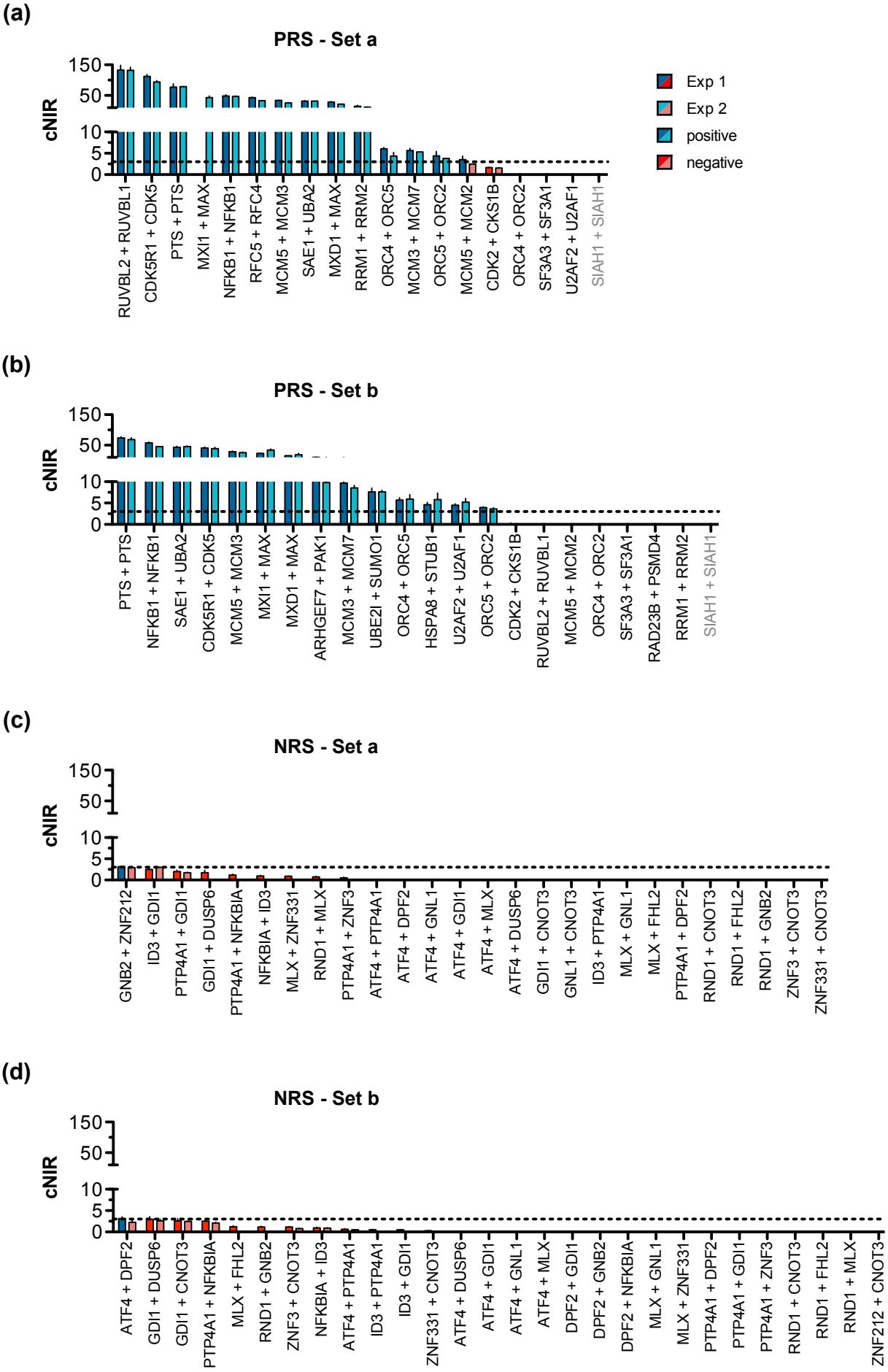
(a)
PRS - Set a
cNIR
150
50
10
5
0
Exp 1
Exp 2
positive
negative
RUVBL2 + RUVBL1
CDK5R1 + CDK5
PTS + PTS
MXI1 + MAX
NFKB1 + NFKB1
RFC5 + RFC4
MCM5 + MCM3
SAE1 + UBA2
MXD1 + MAX
RRM1 + RRM2
ORC4 + ORC5
MCM3 + MCM7
ORC5 + ORC2
MCM5 + MCM2
CDK2 + CKS1B
ORC4 + ORC2
SF3A3 + SF3A1
U2AF2 + U2AF1
SIAH1 + SIAH1
(b)
PRS - Set b
cNIR
150
50
10
5
0
PTS + PTS
NFKB1 + NFKB1
SAE1 + UBA2
CDK5R1 + CDK5
MCM5 + MCM3
MXI1 + MAX
MXD1 + MAX
ARHGEF7 + PAK1
MCM3 + MCM7
UBE2I + SUMO1
ORC4 + ORC5
HSPA8 + STUB1
U2AF2 + U2AF1
ORC5 + ORC2
CDK2 + CKS1B
RUVBL2 + RUVBL1
MCM5 + MCM2
ORC4 + ORC2
SF3A3 + SF3A1
RAD23B + PSMD4
RRM1 + RRM2
SIAH1 + SIAH1
(c)
NRS - Set a
cNIR
150
50
10
5
0
GNB2 + ZNF212
ID3 + GDI1
PTP4A1 + GDI1
GDI1 + DUSP6
PTP4A1 + NFKBIA
NFKBIA + ID3
MLX + ZNF331
RND1 + MLX
PTP4A1 + ZNF3
ATF4 + PTP4A1
ATF4 + DPF2
ATF4 + GNL1
ATF4 + GDI1
ATF4 + MLX
ATF4 + DUSP6
GDI1 + CNOT3
GNL1 + CNOT3
ID3 + PTP4A1
MLX + GNL1
MLX + FHL2
PTP4A1 + DPF2
RND1 + CNOT3
RND1 + FHL2
RND1 + GNB2
ZNF3 + CNOT3
ZNF331 + CNOT3
(d)
NRS - Set b
cNIR
150
50
10
5
0
ATF4 + DPF2
GDI1 + DUSP6
GDI1 + CNOT3
PTP4A1 + NFKBIA
MLX + FHL2
RND1 + GNB2
ZNF3 + CNOT3
NFKBIA + ID3
ATF4 + PTP4A1
ID3 + PTP4A1
ID3 + GDI1
ZNF331 + CNOT3
ATF4 + DUSP6
ATF4 + GDI1
ATF4 + GNL1
ATF4 + MLX
DPF2 + GDI1
DPF2 + GNB2
DPF2 + NFKBIA
MLX + GNL1
MLX + ZNF331
PTP4A1 + DPF2
PTP4A1 + GDI1
PTP4A1 + ZNF3
RND1 + CNOT3
RND1 + FHL2
RND1 + MLX
ZNF212 + CNOT3

Figure S4

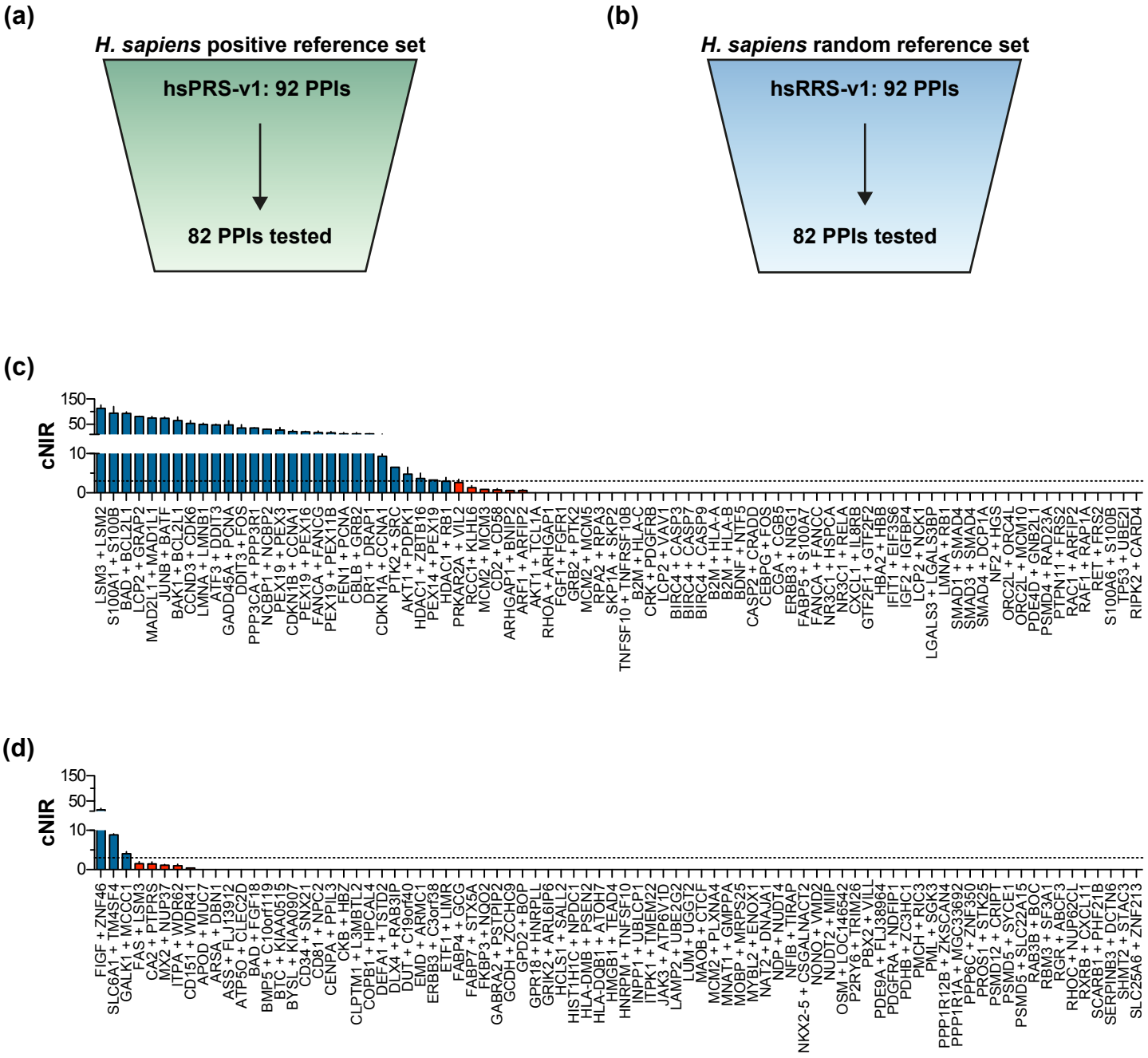
(a)
H. sapiens positive reference set
hsPRS-v1: 92 PPIs
82 PPIs tested
(b)
H. sapiens random reference set
hsRRS-v1: 92 PPIs
82 PPIs tested
(c)
cNIR
150
50
10
0
LSM3 + LSM2
S100A1 + S100B
BAD + BCL2L1
LCP2 + GRAP2
MAD2L1 + MAD1L1
JUNB + BATF
BAK1 + BCL2L1
CCND3 + CDK6
LMNA + LMNB1
ATF3 + DDIT3
GADD45A + PCNA
DDIT3 + FOS
PPP3CA + PPP3R1
NCBP1 + NCBP2
PEX19 + PEX3
CDKN1B + CCNA1
PEX19 + PEX16
FANCA + FANCG
PEX19 + PEX11B
FEN1 + PCNA
CBLB + GRB2
DR1 + DRAP1
CDKN1A + CCNA1
PTK2 + SRC
AKT1 + PDPK1
HDAC1 + ZBTB16
PEX14 + PEX19
HDAC1 + RB1
PRKAR2A + VIL2
RCC1 + KLHL6
MCM2 + MCM3
CD2 + CD58
ARHGAP1 + BNIP2
ARF1 + ARFIP2
AKT1 + TCL1A
RHOA + ARHGAP1
FGF1 + FGFR1
GRB2 + PTK2
MCM2 + MCM5
RPA2 + RPA3
SKP1A + SKP2
TNFSF10 + TNFRSF10B
B2M + HLA-C
CRK + PDGFRB
LCP2 + VAV1
BIRC4 + CASP3
BIRC4 + CASP7
BIRC4 + CASP9
B2M + HLA-A
B2M + HLA-B
BDNF + NTF5
CASP2 + CRADD
CEBPG + FOS
CGA + CGB5
ERBB3 + NRG1
FABP5 + S100A7
FANCA + FANCC
NR3C1 + HSPCA
NR3C1 + RELA
CXCL1 + IL8RB
GTF2F1 + GTF2F2
HBA2 + HBB
IFIT1 + EIF3S6
IGF2 + IGFBP4
LCP2 + NCK1
LGALS3 + LGALS3BP
LMNA + RB1
SMAD1 + SMAD4
SMAD3 + SMAD4
SMAD4 + DCP1A
NF2 + HGS
ORC2L + ORC4L
ORC2L + MCM10
PDE4D + GNB2L1
PSMD4 + RAD23A
PTPN11 + FRS2
RAC1 + ARFIP2
RAF1 + RAP1A
RET + FRS2
S100A6 + S100B
TP53 + UBE2I
RIPK2 + CARD4
(d)
cNIR
150
50
10
0
FIGF + ZNF46
SLC6A1 + TM4SF4
GALK1 + MCCC1
FAS + LSM3
CA2 + NUP37
MX2 + WDR62
ITPA + WDR41
CD151 + APOD
APOD + MUC7
ARSA + DBN1
ASS + FLJ13912
ATP5O + CLEC2D
BAD + FGF18
BMP5 + C10orf119
BTC + KIAA0515
BYSL + KIAA0907
CD34 + SNX21
CD81 + NPC2
CENPA + PPIL3
CKB + HBZ
CLPTM1 + L3MBTL2
COPB1 + HPCAL4
DEFA1 + TSTD2
DLX4 + RAB3IP
DUT + C19orf40
EMD + ARMC1
ERBB3 + C3orf38
ETF1 + LIMR
FABP4 + GCG
FABP7 + STX5A
FKBP3 + NQO2
GABRA2 + PSTPIP2
GCDH + ZCCHC9
GPD2 + BOP
GPR18 + HNRPLL
GRIK2 + ARL6IP6
HCLS1 + SALL2
HIST1H1C + NPDC1
HLA-DMB + PSEN2
HLA-DQB1 + ATOH7
HMGB1 + TEAD4
HNRPM + TNFSF10
INPP1 + UBLCP1
ITPK1 + TMEM22
JAK3 + ATP6V1D
LAMP2 + UBE2G2
LUM + UGGT2
MAOB + CTCF
MCM2 + PLXNA4
MNAT1 + GMPPA
MOBP + MRPS25
MYBL2 + ENOX1
NAT2 + DNAJA1
NDP + NUDT4
NFIB + TIRAP
NKX2-5 + CSGALNACT2
NONO + VMD2
NUDT2 + MIIP
OSM + LOC146542
P2RY6 + TRIM26
PBX2 + VILL
PDE9A + FLJ38964
PDGFRA + NDFIP1
PDHB + ZC3HC1
PMCH + RIC3
PML + SGK3
PPP1R12B + ZKSCAN4
PPP1R1A + MGC33692
PPP6C + ZNF350
PROS1 + STK25
PSMD12 + CRIP1
PSMD5 + SYCE1
PSMD5 + SLC22A15
RAB3B + BOC
RBM3 + SF3A1
RGR + ABCF3
RHOC + NUP62CL
RXRB + CXCL11
SCARB1 + PHF21B
SERPINB3 + DCTN6
SHMT2 + STAC3
SLC25A6 + ZNF213

Figure S5

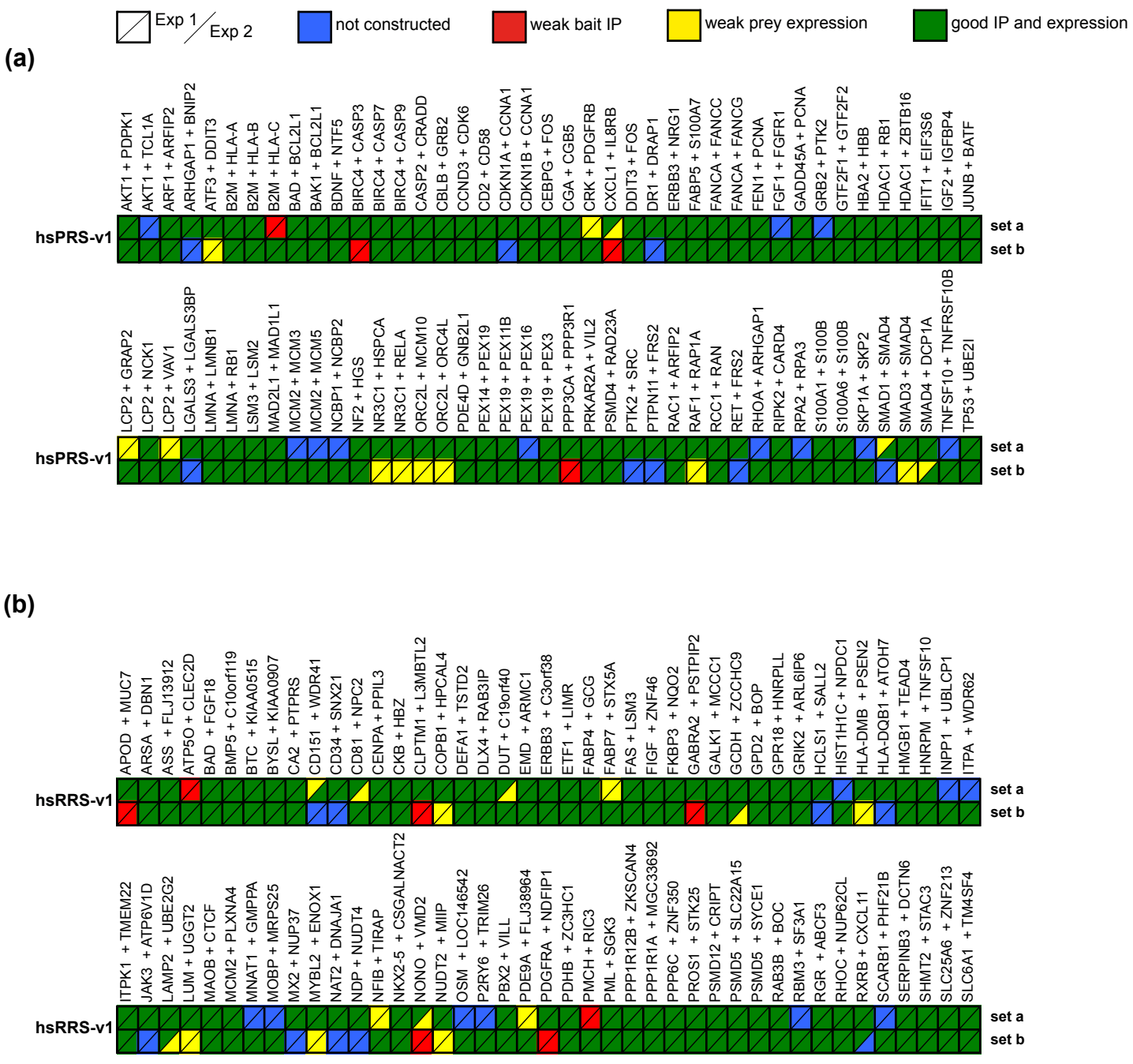
Exp 1
Exp 2
not constructed
weak bait IP
weak prey expression
good IP and expression
(a)
hsPRS-v1
set a
set b
AKT1 + PDPK1
AKT1 + TCL1A
ARF1 + ARFIP2
ARHGAP1 + BNIP2
ATF3 + DDIT3
B2M + HLA-A
B2M + HLA-B
B2M + HLA-C
BAD + BCL2L1
BAK1 + BCL2L1
BDNF + NTF5
BIRC4 + CASP3
BIRC4 + CASP7
BIRC4 + CASP9
CASP2 + CRADD
CBLB + GRB2
CCND3 + CDK6
CD2 + CD58
CDKN1A + CCNA1
CDKN1B + CCNA1
CEBPG + FOS
CGA + CGB5
CRK + PDGFRB
CXCL1 + IL8RB
DDIT3 + FOS
DR1 + DRAP1
ERBB3 + NRG1
FABP5 + S100A7
FANCA + FANCC
FANCA + FANCG
FEN1 + PCNA
FGF1 + FGFR1
GADD45A + PCNA
GRB2 + PTK2
GTF2F1 + GTF2F2
HBA2 + HBB
HDAC1 + RB1
HDAC1 + ZBTB16
IFIT1 + EIF3S6
IGF2 + IGFBP4
JUNB + BATF
hsPRS-v1
set a
set b
LCP2 + GRAP2
LCP2 + NCK1
LCP2 + VAV1
LGALS3 + LGALS3BP
LMNA + LMNB1
LMNA + RB1
LSM3 + LSM2
MAD2L1 + MAD1L1
MCM2 + MCM3
MCM2 + MCM5
NCBP1 + NCBP2
NF2 + HGS
NR3C1 + HSPCA
NR3C1 + RELA
ORC2L + MCM10
ORC2L + ORC4L
PDE4D + GNB2L1
PEX14 + PEX19
PEX19 + PEX11B
PEX19 + PEX16
PEX19 + PEX3
PPP3CA + PPP3R1
PRKAR2A + VIL2
PSMD4 + RAD23A
PTK2 + SRC
PTPN11 + FRS2
RAC1 + ARFIP2
RAF1 + RAP1A
RCC1 + RAN
RET + FRS2
RHOA + ARHGAP1
RIPK2 + CARD4
RPA2 + RPA3
S100A1 + S100B
S100A6 + S100B
SKP1A + SKP2
SMAD1 + SMAD4
SMAD3 + SMAD4
SMAD4 + DCP1A
TNFSF10 + TNFRSF10B
TP53 + UBE2I
(b)
hsRRS-v1
set a
set b
APOD + MUC7
ARSA + DBN1
ASS + FLJ13912
ATP5O + CLEC2D
BAD + FGF18
BMP5 + C10orf119
BTC + KIAA0515
BYSL + KIAA0907
CA2 + PTPRS
CD151 + WDR41
CD34 + SNX21
CD81 + NPC2
CENPA + PPIL3
CKB + HBZ
CLPTM1 + L3MBTL2
COPB1 + HPCAL4
DEFA1 + TSTD2
DLX4 + RAB3IP
DUT + C19orf40
EMD + ARMC1
ERBB3 + C3orf38
ETF1 + LIMR
FABP4 + GCG
FABP7 + STX5A
FAS + LSM3
FIGF + ZNF46
FKBP3 + NQO2
GABRA2 + PSTPIP2
GALK1 + MCCC1
GCDH + ZCCHC9
GPD2 + BOP
GPR18 + HNRPLL
GRIK2 + ARL6IP6
HCLS1 + SALL2
HIST1H1C + NPDC1
HLA-DMB + PSEN2
HLA-DQB1 + ATOH7
HMGB1 + TEAD4
HNRPM + TNFSF10
INPP1 + UBLCP1
ITPA + WDR62
hsRRS-v1
set a
set b
ITPK1 + TMEM22
JAK3 + ATP6V1D
LAMP2 + UBE2G2
LUM + UGGT2
MAOB + CTCF
MCM2 + PLXNA4
MNAT1 + GMPPA
MOBP + MRPS25
MX2 + NUP37
MYBL2 + ENOX1
NAT2 + DNAJA1
NDP + NUDT4
NFIB + TIRAP
NKX2-5 + CSGALNACT2
NONO + VMD2
NUDT2 + MIIP
OSM + LOC146542
P2RY6 + TRIM26
PBX2 + VILL
PDE9A + FLJ38964
PDGFRA + NDFIP1
PDHB + ZC3HC1
PMCH + RIC3
PML + SGK3
PPP1R12B + ZKSCAN4
PPP1R1A + MGC33692
PPP6C + ZNF350
PROS1 + STK25
PSMD12 + CRIPT
PSMD5 + SLC22A15
PSMD5 + SYCE1
RAB3B + BOC
RBM3 + SF3A1
RGR + ABCF3
RHOC + NUP62CL
RXRB + CXCL11
SCARB1 + PHF21B
SERPINB3 + DCTN6
SHMT2 + STAC3
SLC25A6 + ZNF213
SLC6A1 + TM4SF4

Figure S6